TECHNICAL UNIVERSITY OF LIBEREC

Faculty of Mechatronics, Informatics and Interdisciplinary Studies Study Program:
Environmental Engineering

THESIS FOR THE STATE DOCTORAL EXAMINATION

Highly efficient membrane development for advanced wastewater treatment system

Author: Hadi Taghavian, M.Sc. (hadi.taghavian@tul.cz)
Supervisor: prof. Dr. Ing. Miroslav Černík, CSc. (Miroslav.Cernik@tul.cz)
Co-supervisor: Ing. Mgr. Lukáš Dvořák, Ph.D. (Lukas.dvorak@tul.cz)

Contents

List of Abbreviations

PDA	Polydopamine
DA	Decanoic acid
PI	Polyimide
WCA	Water contact angle
PVDF	polyvinylidene fluoride
EPS	extracellular polymeric substances
PTFE	Polytetrafluoroethylene
PVC	Polyvinylidene fluoride
MOF	Metal-organic framework
PPSU	Polyphenylsulfone
PET	polyethylene terephthalate
Si-QAC	3-(trimethoxysilyl) propyldimethyloctadecyl ammonium chloride
FE-SEM	field emission-scanning electron microscopy
IPA	isopropanol
EDS	energy dispersive X-ray spectroscopy
FT-IR	Fourier transform infrared spectroscopy
XRD	X-ray diffraction
AFM	atomic force microscopy
RMS	root mean square
TMP	transmembrane pressure
E. coli	Escherichia coli
CFU	Colony forming unit
HF	Hollow fiber
DI	Deionized
AS	Activated sludge
ZnO	Zinc oxide

1. Introduction

With the rising global population and increasing demand for water and energy resources, water scarcity has become a pressing issue intensified by factors like climate change and reduced rainfall. These challenges underscore the critical need for advanced wastewater treatment technologies that ensure a sustainable water supply. Conventional wastewater treatment techniques vary depending on factors such as the organic content in the inflow, biomass concentrations, quality requirements of the treated water, and constraints on energy and land use. In recent years, membrane technology has gained substantial attention and has been commercially applied to separate components from mixed solutions due to its advantages, including low initial investment, low energy and operational costs, high capacity, compact design, and high removal efficiency, yielding high-quality effluent [1], [2], [3].

Despite significant advancements in membrane applications, improvements are still required to address challenges that limit widespread use. Fouling due to pollutants and deposits on the membrane surface, including inorganic residues, organic compounds, and biological substances, leads to pore blockages, reduced hydraulic efficiency, and higher operational costs [4], [5], [6], [7], [8]. Efforts to manage fouling, such as backwashing, chemical cleaning, and air bubble induction, aim to control fouling and restore initial flux in order to enhance the potential capability of membranes as an alternative to traditional clarifiers [4]. However, these methods consume energy, increase costs, and reduce membrane lifespan.

Synthetic organic polymers, known for their stability, were widely used for the fabrication of membranes [8], [9]. However, their hydrophobic nature attracts proteins, fatty acids, and microorganisms, which contribute to fouling by attaching to or trapping in the membrane pores [10], [11]. This attraction between the hydrophobic membrane surface and hydrophobic foulants accelerates fouling and presents an ongoing challenge [11].

Another significant factor in fouling is biofilm formation, driven by bacterial attraction to the membrane surface. Membrane bioreactor (MBR) systems, which often operate with high sludge concentrations and suspended solids, provide ample substrates for bacterial growth [8]. This environment encourages the production of extracellular polymeric substances (EPS), which help bacteria adhere to the membrane, forming biofilms that clog pores, reduce permeability, and increase fouling rates [12]. Surface modification by integrating inorganic nanoparticles into membranes can impart antimicrobial properties and enhance hydrophobicity/hydrophilicity tramsformation, providing a promising solution for biofilm mitigation [13], [14].

In addition, operational parameters play a critical role in managing fouling. Even surface-modified membranes are susceptible to fouling if used under severe conditions. Critical flux is defined as the flux above which membrane fouling accelerates [15], [16]. Since each membrane's critical flux depends on specific surface modification parameters, its evaluation is essential. Effective control of operational conditions, such as aeration and flux below the critical flux, along with tailored membrane properties, is crucial to reducing fouling in MBRs [15], [16]. In summary, minimizing biofouling and optimizing MBR performance requires a comprehensive approach that considers membrane surface properties and operational conditions.

Considering that fouling is primarily influenced by the interaction between the membrane's intrinsic properties [10], [11], characteristics of the fouling substances [17], [18], [19], and operational conditions [15], [16], this study focused on modifying membrane surfaces using various techniques and determining the optimal modification conditions to achieve enhanced performance. By applying these surface modifications and optimizing performance parameters, this research aims to achieve a sustainable balance between high contaminant removal efficiency and reduced fouling, ultimately extending membrane lifespan and reducing operational costs. Employing an eco-friendly surface modification approach, combined with evaluation of optimum flux for operation, this study addresses both the surface characteristics and operating conditions needed to enhance the performance of PES hollow fiber (HF) membranes in advanced wastewater treatment applications.

2. Research objectives

This research intends to modify the surface of membranes to repel or reduce interactions between the membrane surface and microorganisms, dissolved organic matter, suspended solids, proteins, and particulate particles and enhance membrane performance. The focus is on optimizing surface characteristics, hydrophobicity/hydrophilicity transformation, and bacterial resistivity. Accordingly, various surface modifications have been investigated to achieve highly efficient membranes for advanced wastewater treatment systems. This study focuses on three key methodologies: (I) superhydrophobic and (II) superhydrophilic surface modifications incorporated inorganic biocide NPs, as well as (III) performance improvement.

(I) Superhydrophobic Surface Coating: Similar to the nature-inspired superhydrophobicity of the lotus leaves, which enables them to repel dirt from the surface, the first technique involves applying a superhydrophobic coating to woven polyester fabric, transforming it into a selective membrane. The primary hypothesis is that this coating, designed to be versatile and easily applicable to various membrane surfaces, enhances selective permeance while providing antibacterial properties. Through incorporation with NPs, it is intended to obtain bacterial repulsive properties.

(II) Superhydrophilic Surface Modification: The second technique involves the superhydrophilic surface modification of membranes. This approach minimizes fouling, enhances water permeability during filtration, and significantly improves overall process efficiency. Additionally, the integration of nanoparticles can improve bacterial resistivity, making the surface-modified membranes more effective and durable for advanced filtration applications.

(III) Performance improvement: The third technique emphasizes finding the optimized membrane flux through the evaluation of critical flux. This optimized flux during membrane performance in a bioreactor directly impacts the modified membranes' permeability, fouling rate, and overall biofouling reduction.

Together, this study aims to comprehensively explore various aspects of membrane surface modifications, taking one step forward in advancing membrane technology for wastewater treatment applications.

3. State of the art

Membrane fouling, which is significantly impacted by the interaction between a membrane's intrinsic properties and the characteristics of fouling substances, has driven the development of surface modification as a promising solution [4], [5], [6]. A variety of surface modification techniques have been explored in membrane research, with numerous studies focusing on reducing membrane fouling and enhancing their sustainable performance [10], [11]. To achieve these goals, various physicochemical methods have been employed, including surface polymerization and coating [11], incorporation of metal-organic frameworks (MOFs) [20], and nanoparticles (NPs) immobilization [21], [22]. However, these techniques share several key requirements. First, modifications must avoid blocking membrane pores. Second, the modified layer and immobilized nanoparticles must exhibit stability. Lastly, the modification process should ideally utilize eco-friendly methods to prevent the release of toxic materials during or after treatment, thereby minimizing secondary environmental concerns. Recent studies have focused on four primary strategies to enhance membrane performance: (i) surface modification to increase hydrophobicity, (ii) superhydrophilic surface modification, (iii) the incorporation of inorganic antibacterial agents to inhibit biofilm formation, and (iv) the optimization of operational parameters.

(i) Superhydrophobic surface modification

Superhydrophobic surface modification has been increasingly utilized in membranes for applications in the water treatment industry, particularly those concerned with mixtures of oil or organic solvents in water. It was demonstrated that a selective membrane can be achieved by coating cotton fabric with reduced graphene oxide (rGO), resulting in a water contact angle (WCA) exceeding 150° and achieving over 97% separation efficiency for oils [23]. Ma et al. explored the significant potential of surface-modified polyimide (PI) nanofibrous membranes coated with decanoic acid (DA) combined with TiO_2 and silica NPs [24]. This modification created a superhydrophobic surface with a WCA exceeding 155°, achieving approximately 99% separation efficiency in oil-water separation [24]. Similarly, Thabit et al. investigated the surface bonding of Fe^{3+}/stearic acid onto cotton fabric to create a superhydrophobic membrane with a WCA of approximately 156° [25]. The modified membrane demonstrated selective separation efficiencies exceeding 95% for light oils and 98% for heavy oils [25]. The mechanical strength, reusability, and shelf-life of superhydrophobic membranes play vital roles in defining their applications. However, a significant drawback is their limited resistance to fouling, which decreases membrane efficiency and shortens operational life. Accordingly, in the first part of this study, we tried to develop a versatile coating with the capability of easily applying on different substrates and turning them into bacteria-resistant selective membranes.

Although superhydrophobic membrane surfaces offer exceptionally low surface tension, which contributes to their non-stick properties against particulate particles, this characteristic also prevents the surface from wetting, thereby limiting water permeability. Consequently, this modification approach is particularly suited for the selective separation of organic solvents and addressing oil spills in industrial wastewater treatment. Additionally, it shows promising potential for enhancing the performance of desalination membranes.

(ii) Superhydrophilic surface modification

Superhydrophilic surface modification of membranes has garnered significant attention as a solution to membrane fouling. This modification technique arises because the hydrophobic nature of polymeric membranes promotes the adsorption of proteins, fatty acids, and many filamentous microorganisms, contributing to fouling [10], [11]. These foulants primarily exhibit hydrophobic characteristics, which interact strongly with the hydrophobic surface of organic membranes [17], [18], [19]. This interaction enhances their adhesion to the membrane surface or entrapment within the pores, accelerating the fouling process [11].

Recent studies have suggested that membranes with hydrophilic surface modifications resisted fouling more effectively. Galiano et al. enhanced the hydrophilicity of a polyethersulfone (PES) membrane by applying a polymerized surfactant coating, improving its resistance to fouling by organic textile dyes in a bioreactor [12]. Similarly, Johnson et al. found that hydrophobic membranes used in wastewater treatment displayed higher fouling potential [26]. In addition, superhydrophilic surface modification has shown the potential to enhance flux recovery by approximately 90% after coating PTFE flat-sheet membranes with PDA [27]. Similarly, applying a PDA/polyethyleneimine (PEI) coating to a PTFE HF membrane can render its surface superhydrophilic, achieving a WCA of 0° and enhancing water permeation flux [10]. Zhang et al. demonstrated the benefits of hydrophilizing PTFE flat-sheet membranes by reducing the WCA to approximately 60° using a triple coating layer of PDA/Ag NPs/PDA, which resulted in a 325.7% improvement in flux [28]. Consequently, hydrophilic surface treatment of membranes has become a key strategy, especially in systems with high levels of hydrophobic pollutants.

(iii) Nanoparticle incorporation

While hydrophilic/hydrophobic surface modification can reduce membrane fouling in various applications, it is insufficient to fully address bacterial growth and biofilm formation. The need for an effective biocide remains critical. Immobilizing inorganic NPs with proven antimicrobial properties onto the membrane surface has gained significant attention due to its efficiency and long-lasting performance. Immobilized NPs provide a long-lasting antibacterial effect since they remain bound to the membrane and continue to interact with microorganisms. In addition, NPs can be immobilized on the surface without altering the porosity, chemical resistivity, and mechanical strength of the membrane. This approach relies on robust immobilization techniques that ensure stability and durability, effectively mitigating biofouling problems [20], [21], [22]. Zolghadr et al. successfully *in situ* grafted Ag-MOFs onto a PDA-coated polyvinylidene fluoride (PVDF) membrane, resulting in an anti-biofouling surface with demonstrated antimicrobial activity against *Escherichia coli (E. coli)* and *Staphylococcus aureus* [20]. The Fe_3O_4/PDA/Ag composite NPs demonstrated a positive impact on biofouling control of the polyvinyl chloride (PVC) membrane, achieving an impressive 70% flux recovery and showcasing their effectiveness in maintaining membrane performance [22]. Pakizeh et al. demonstrated that integrating TiO_2 NPs and PDA onto the polyphenylsulfone (PPSU) membrane surface substantially improved flux recovery from 60% to 87% while enhancing antifouling properties and dye removal efficiency [21].

(iv) operational conditions optimizations

Performance under optimal operating conditions is another critical factor influencing membrane fouling. MBR systems are designed to operate with high biomass concentrations, which naturally elevate fouling rates. However, fouling can be mitigated by carefully managing operational parameters to reduce the accumulation of foulants on the membrane surface. Key strategies to address membrane fouling include optimizing operational conditions such as aeration flow rate, aeration timing, diffuser positioning, backwashing, relaxation intervals, and flux regulation during system operation. Fu et al. examined the effects of aeration flow rate, position, and time on membrane fouling under various operational conditions [29]. Their findings demonstrated that optimizing these parameters could effectively minimize membrane fouling in MBR systems and control energy consumption per unit of effluent [29]. It was demonstrated that optimizing operational parameters in MBR, such as backwashing and relaxation durations, is crucial for controlling membrane fouling, with backwashing duration showing the greatest impact [30]. By employing optimization methods, the combined effects of parameters can be fine-tuned to enhance MBR performance and minimize fouling effectively [30]. Monclus et al. demonstrated that optimizing filtration flux is one of the most effective strategies for mitigating membrane fouling during MBR operation [15], [16]. It was proven that operating submerged membranes below the critical flux (J_c) which is the threshold at which fouling significantly accelerates, can effectively minimize the fouling rate during performance [15], [16].

While each of the four primary strategies provides distinct benefits for addressing biofouling, achieving optimal membrane performance in water treatment often requires simultaneously combining multiple modification strategies. However, modifying one factor can sometimes adversely impact another. Therefore, we aim to address these limitations and propose optimal solutions for the efficient development of membranes tailored to advanced wastewater treatment systems.

4. Experimental work

The experimental section of this study is primarily based on two published articles and one proceeding paper. It is divided into three main chapters, each providing a detailed methodological description of the experiments, results, and a summary discussion.

- **Chapter 1: Superhydrophobic surface modification**
  This chapter focuses on the first superhydrophobic surface modification strategy and the third strategy involving NPs incorporation, as outlined in the published article [31]. A novel biomimetic coating, inspired by the hydrophobic properties of lotus leaves, was developed to enhance the separation performance of polyethylene terephthalate (PET)

fabric surfaces. This approach employs a hierarchical composition of nanocomposite coating: polydopamine (PDA), in-situ synthesized ZnO NPs, and a non-fluorinated silane layer. The modification technique successfully met key requirements, including maintaining non-blocked membrane pores, achieving robust nanocomposite immobilization with physicochemical stability, and employing an eco-friendly procedure.

- **Chapter 2: Superhydrophilic surface modification**
  This chapter utilizes the second superhydrophilic surface modification strategy combined with the third strategy involving NP incorporation, in line with the published article [32]. The study introduces a facile surface modification methodology suitable for various HF membranes, including PTFE, effectively transforming them into ideal candidates for wastewater treatment applications.

- **Chapter 3: Fouling rate and critical flux evaluation of the modified membranes**
  The third chapter focuses on the fourth strategy, which involves evaluating the effect of modification parameters on the critical flux, which is essential for achieving optimal membrane performance.

4.1. Chapter 1: **Superhydrophobic surface modification**

4.1.1. Materials and method

4.1.1.1. Surface coating methodology

The superhydrophobic modification of PET fabric (Licolor, a.s., Czechia) was conducted through a three-step hierarchical process. First, the fabric was coated with PDA via oxidative polymerization by immersing it in a dopamine hydrochloride (Alfa Aesar, USA) solution of 2.0 $mg\cdot mL^{-1}$, Tris buffer (Penta, Czechia), at pH 8.5, and shaking at 100 rpm for 24 hours at room temperature. The resulting PDA-coated samples (PDA@PET) were rinsed with deionized (DI) water and dried. Next, in-situ synthesis of zinc oxide (ZnO) NPs was performed by immersing PDA@PET in zinc acetate (Merck, Germany) solutions (10 - 40 $mmol\cdot L^{-1}$), followed by vigorous stirring at 80˚C with Tris-base addition to achieve a pH of 9. The ZnO/PDA@PET samples were rinsed with DI water and dried at 60˚C for 1 hour. Finally, silanization was carried out by soaking ZnO/PDA@PET in a 6% (v/v) solution of 3-(trimethoxysilyl) propyldimethyloctadecyl ammonium chloride (Si-QAC; Merck, Germany) in ethanol (pH ~4) for 24 hours with shaking at 150 rpm. The samples were dried at 105˚C for 1 hour, yielding superhydrophobic membranes. For comparison, unmodified PET was coated with Si-QAC alone to evaluate hydrophilicity.

4.1.1.2. Surface Morphology and Chemical Composition

The surface morphology and elemental composition of pristine and modified PET samples were analyzed using field emission-scanning electron microscopy (FE-SEM) and energy dispersive X-ray spectroscopy (EDS). To avoid charging effects during SEM imaging, a 2 nm platinum conductive coating was applied. Fourier transform infrared spectroscopy (FT-IR) was employed to identify surface chemical bonds, while X-ray diffraction (XRD) provided insights into the structural composition of the modified samples using Cu Kα1 radiation (40 kV, 30 mA, λ = 0.1789 nm). Surface roughness was measured via atomic force microscopy (AFM) over a scanned area of 2.5 μm × 2.5 μm, with results expressed as root mean square (RMS) values calculated from triplicate measurements.

4.1.1.3. Antimicrobial Assessments

The antimicrobial performance of Si-QAC/ZnO/PDA@PET membranes, modified with varying ZnO NP concentrations, was assessed qualitatively following AATCC method 147. Tests were conducted using gram-positive *Staphylococcus sp*. (CCM 2446) and gram-negative *E. coli* (CCM 7395), obtained from the Czech Collection of Microorganisms at Masaryk University, Brno. A bacterial suspension (105 cells·mL-1) was prepared using a Densi-La-Meter® II (Erba Lachema, Czechia) and diluted in series (non-diluted, 10×, 100×, and 1000×). Stripes of these suspensions were streaked on plate-count agar, with membrane samples (1 × 4.5 cm) placed perpendicular to the bacterial strikes. Following 48 hours of incubation at 37°C, the contact zone, the distance between the edge of the membranes and bacterial growth, was observed to evaluate bacterial repulsion. Growth beneath the membrane samples was also examined. Minimal bacterial growth in the contact zone indicated effective antibacterial activity. All experiments were conducted in duplicate to ensure reliability.

4.1.1.4. Superhydrophobicity Analysis and Water-Solvent Separation Performance

Superhydrophobicity was characterized by WCA (Kruss, model DSA30E, Germany) measurements and roll-off angles (Laserliner, model ARCOMASTER 40, Germany). Durability was tested via mechanical abrasion (sandpaper method), repeated cleaning cycles (ISO 105 C06, B1M), exposure to acidic and alkaline solutions (pH 1 and pH 13), and ultraviolet radiation. The self-cleaning ability of the superhydrophobic PET samples was assessed by sprinkling 0.5 g of dyed microfibers on the surface and rolling water droplets over them, recorded with a digital camera. Water droplet bouncing was captured using a high-speed camera (Olympus i-SPEED 3, Japan) at 5000 frame·s^{-1}.

The water-organic solvent separation efficiency of Si-QAC/ZnO/PDA@PET membranes was tested using solvents like n-hexane, toluene, chloroform, and petroleum ether (all supplied by Merck, Germany), stained with Oil Red O for visual clarity. Membranes were fixed onto a glass flask, and solvent-water mixtures were filtered, allowing only solvents to pass through while retaining water. The separation efficiency was calculated by volumetric measurements, confirming the membranes' effectiveness for practical applications.

4.1.2. Results and discussion

4.1.2.1. Synthesis mechanism

The formation of superhydrophobic surfaces involves low surface energy materials and hierarchical nanostructures. Biomimetic self-polymerization of PDA served as a binder to facilitate the immobilization of ZnO NPs and the attachment of Si-QAC on a PET substrate via active -OH and -NH_2 groups. The catechol and amine groups in PDA enabled adhesion to nearly all surfaces, forming nanospheres through oxidative polymerization.

A biological-grade Tris-base solution facilitated the synthesis of ZnO NPs from a $Zn(CH_3COO)_2 \cdot 2H_2O$ solution at elevated temperatures, generating Zn^{2+} and $CH3COO^-$ ions. In an aqueous medium, these ions initiated the formation of ZnO seed lattices [33], [34]. Immersing PDA-coated PET in a solution containing Zn^{2+}, CH_3COO^-, residual $Zn(CH_3COO)_2$, and Tris-base enabled the -OH groups on PDA to react with Zn^{2+} ions and newly formed ZnO seeds, anchoring them to the substrate. The strong interaction between the catechol groups of PDA and ZnO nanoseeds, as reported by Kim et al. [14], combined with post-treatment at 60 ˚C for 1 hour, promoted the growth and stable immobilization of ZnO NPs on the PDA@PET substrate.

The eco-friendly in-situ synthesis of ZnO NPs and PDA coating created micro/nanostructures on the PET surface, further modified with Si-QAC. The trimethoxysilyl group of Si-QAC reacted with PDA’s hydroxyl groups via condensation (silane coupling), releasing methanol [35], [36]. Si-QAC bonded to the substrate through its trimethoxysilyl head, while its long hydrocarbon tails imparted hydrophobic and oleophilic properties. PDA served as a binder and anchor for ZnO NPs and silane agents, enabling the silanization of the ZnO/PDA@PET fabric. This modification produced a superhydrophobic PET fabric with enhanced surface properties. Fig. 1 illustrates the hierarchical nanocomposite coating process.

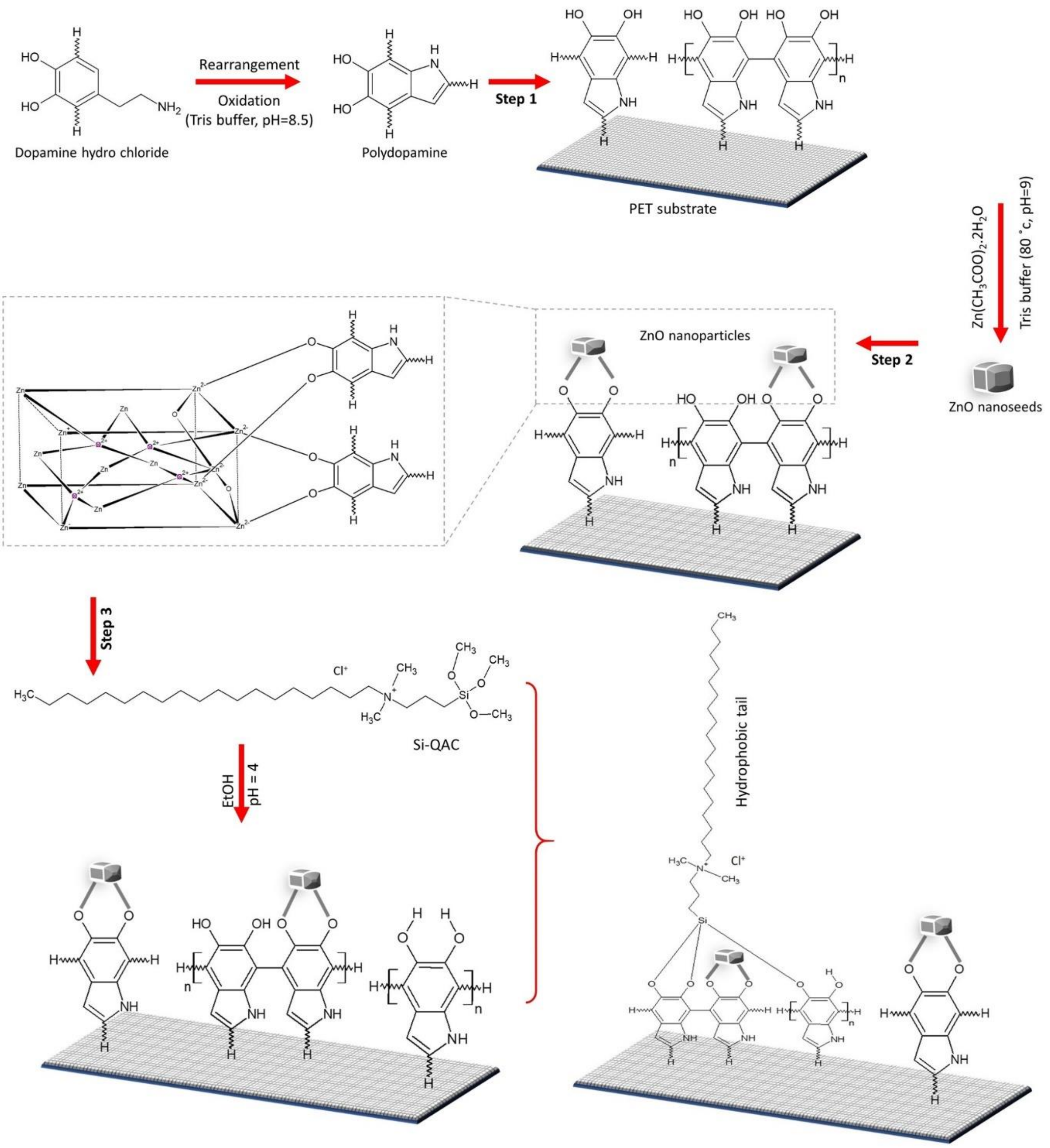

Fig. 1. Schematic representation of the hierarchical nanocomposite coating process on the PET substrate: Step 1- PDA coating, Step 2- in-situ synthesis of ZnO NPs, and Step 3- silanization, leading to the transformation into a superhydrophobic surface.

4.1.2.2. Surface morphology and elemental composition

The SEM images were employed to analyze the morphological changes on the PET surface at each stage of modification, providing insights into the treatment process. Fig. 2, Fig. 3, and Fig. 4 illustrate the SEM images of unmodified PET, PDA@PET, ZnO/PDA@PET, and Si-QAC/ZnO/PDA@PET, respectively. The images revealed a uniform and consistent coating across the PET surface at each modification phase. The untreated PET surface displayed a smooth texture (Fig. 2A, a), while the deposition of PDA nanospheres became evident after the first modification step (Fig. 2B, b). The PDA layer enhanced the surface's hydrophilicity and introduced active sites for the attachment of ZnO NPs, thus improving the performance of the superhydrophobic coating in subsequent modifications.

This study also examined the effect of $Zn(CH_3COO)_2 \cdot 2H_2O$ concentration, used as the precursor for the in-situ synthesis of ZnO NPs. The findings revealed that increasing the zinc acetate concentration (ranging from 10 $mmol \cdot L^{-1}$ to 40 $mmol \cdot L^{-1}$) resulted in a greater quantity and denser distribution of ZnO NPs, as illustrated in Fig. 4a-d. The SEM images clearly show a homogeneous distribution of ZnO NPs on the PDA@PET surface, regardless of the precursor concentration. These observations align with findings by Cheng et al. [37], who noted that higher zinc acetate concentrations significantly influenced the synthesis, leading to a higher yield of ZnO NPs. The results highlight that elevated precursor concentrations accelerate the synthesis rate and promote a denser nanoparticle distribution. This effect is attributed to supersaturation, which facilitates the formation of numerous tiny nuclei, triggering rapid nucleation and synthesis, as corroborated by other studies [38], [39], [40].

The SEM images of silane-treated ZnO/PDA@PET samples, prepared using various zinc acetate concentrations, demonstrated that the PET fibers were uniformly coated with a dense Si-QAC silane layer (Fig. 4). This indicates that the Si-QAC silane exhibited strong compatibility and adherence to the ZnO/PDA@PET surface. Notably, the silane layer exclusively coated the ZnO/PDA@PET fibers without forming a thick, continuous film over the entire surface or significantly altering the overall morphology. As a result, the material's permeability remained unaffected.

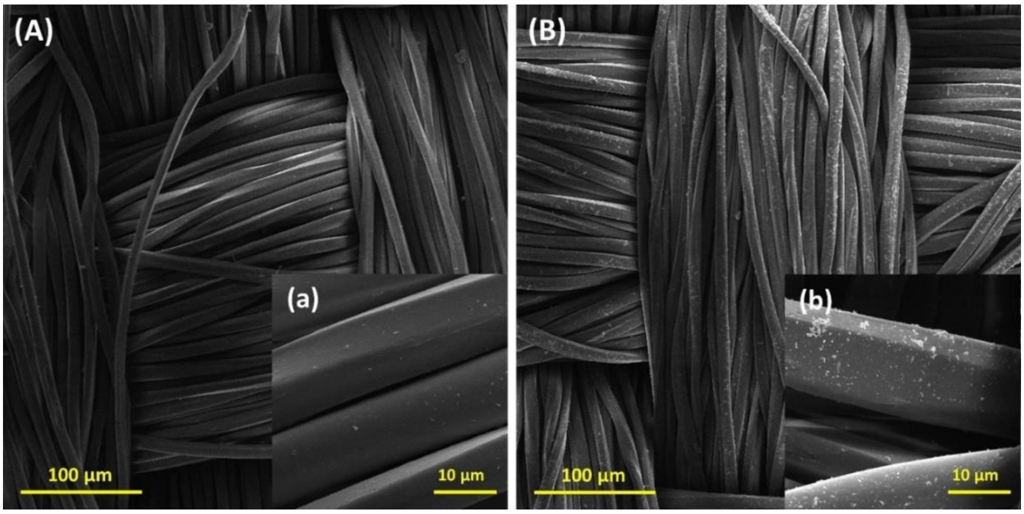

Fig. 2. SEM images of (A) (a) blank PET and (B) (b) PDA-coated PET. Main images (A) and (B) were captured at a magnification of 500 ×, while inset images (a) and (b) were taken at 5,000 ×.

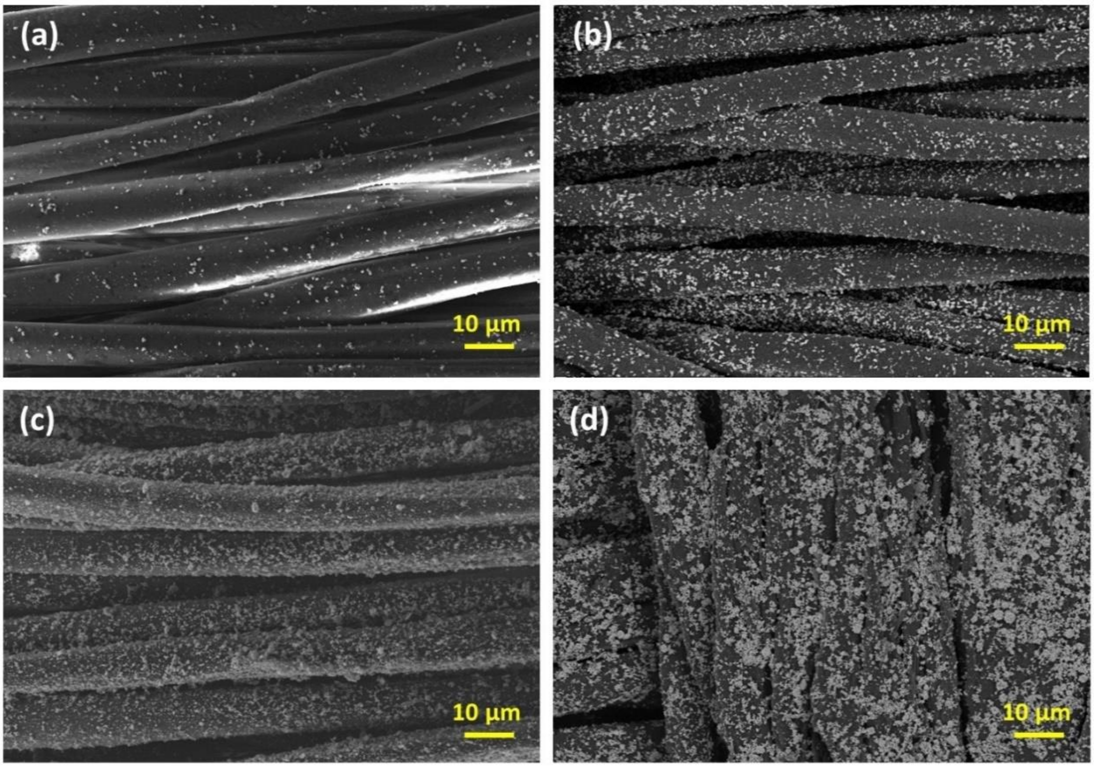

Fig. 3. SEM images (magnification: 1,000×) of ZnO NPs-coated PDA@PET samples prepared using different zinc acetate concentrations: (a) 10 $\text{mmol}\cdot\text{L}^{-1}$, (b) 20 $\text{mmol}\cdot\text{L}^{-1}$, (c) 30 $\text{mmol}\cdot\text{L}^{-1}$, and (d) 40 $\text{mmol}\cdot\text{L}^{-1}$.

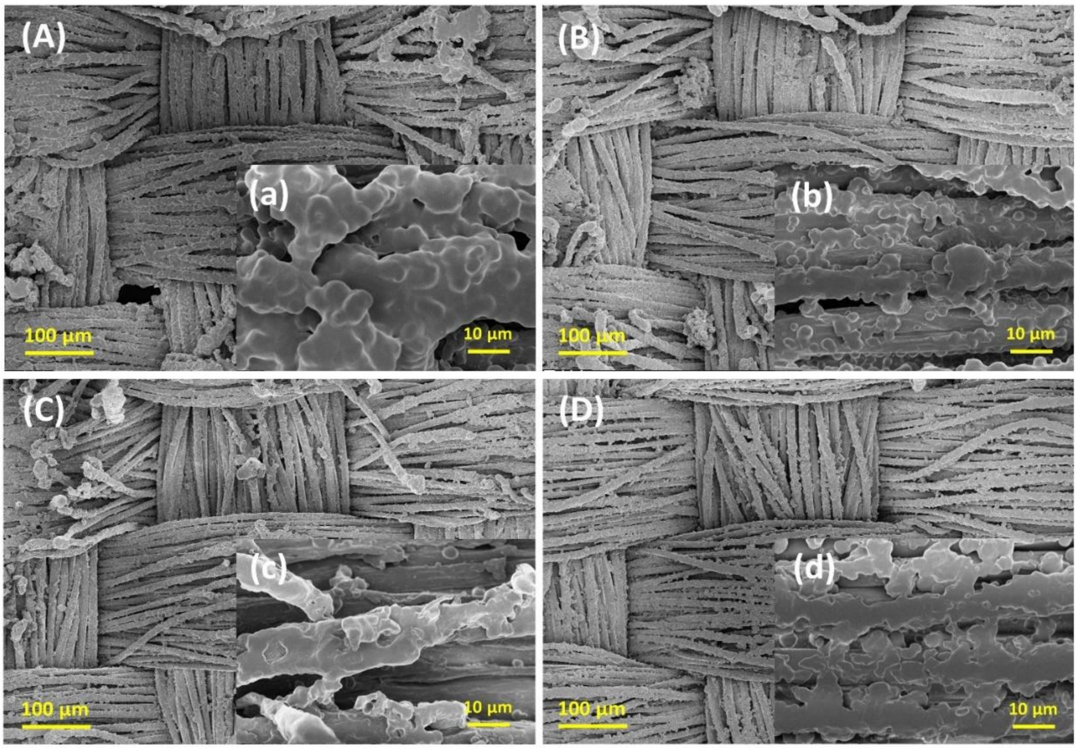

Fig. 4. SEM images of Si-QAC/ZnO/PDA@PET samples synthesized using varying zinc acetate concentrations: (A) (a) 10 $\text{mmol}\cdot\text{L}^{-1}$, (B) (b) 20 $\text{mmol}\cdot\text{L}^{-1}$, (C) (c) 30 $\text{mmol}\cdot\text{L}^{-1}$, and (D) (d) 40 $\text{mmol}\cdot\text{L}^{-1}$. Main images (A) to (D) were captured at a magnification of 150×, while inset images (a) to (d) were taken at 1500×.

The surface elemental composition determined through EDS analysis showed that the relative weight percentages of Zn were 2.94%, 3.78%, 3.81%, and 7.51% for zinc acetate concentrations of 10, 20, 30, and 40 mmol·L^{-1}, respectively. These results align with the SEM observations (Fig. 3a-d), indicating a denser distribution of ZnO NPs with increasing zinc acetate concentration. EDS mapping (Fig. 5) further illustrated the uniform distribution of Zn, along with Si and Cl, identifiers of the Si-QAC layer, demonstrating the homogeneous dispersion of nanoparticles and the silane coating. This confirms the successful surface modification of the PET samples.

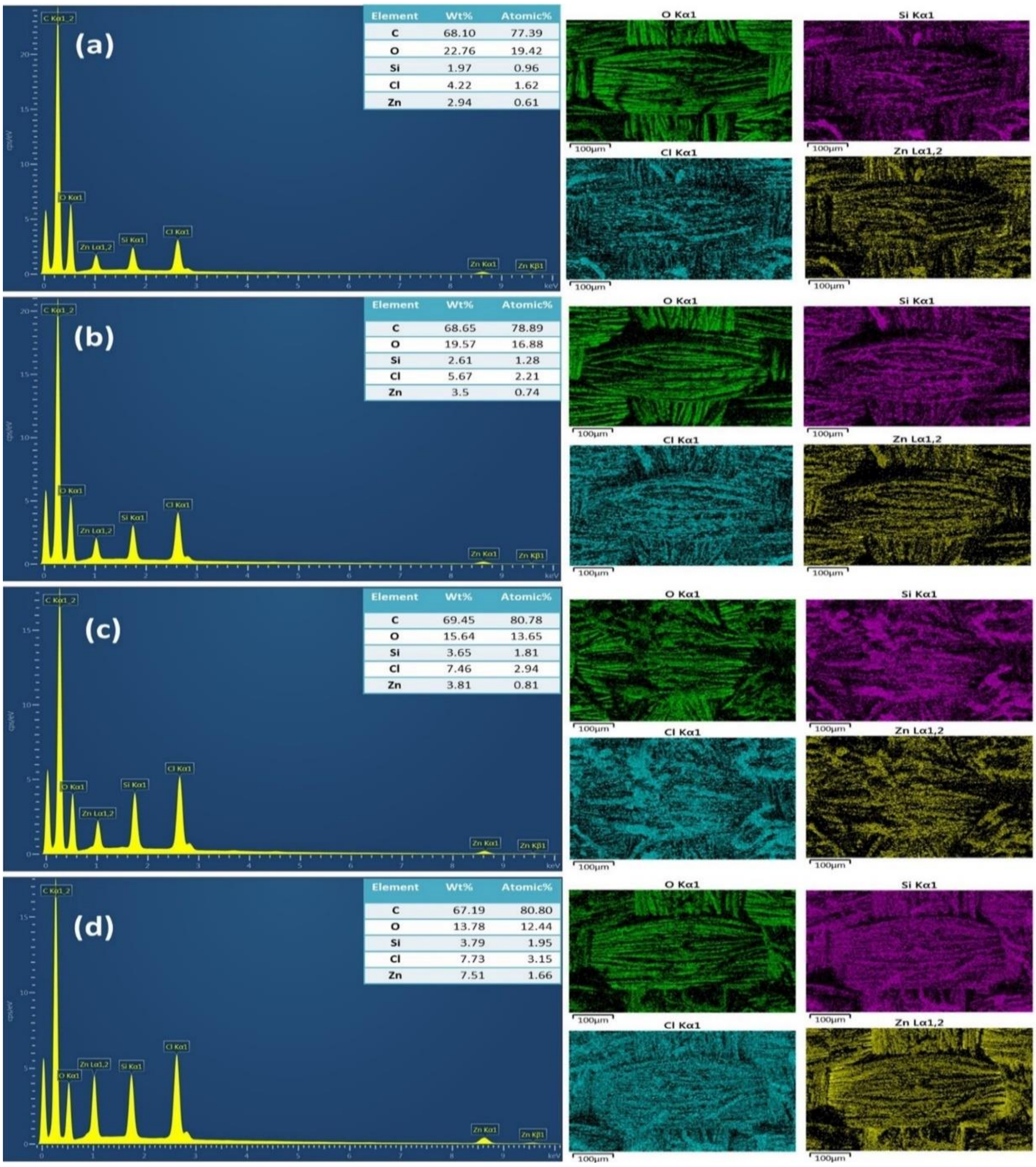

(a)

Element	Wt%	Atomic%
C	68.10	77.39
O	22.76	19.42
Si	1.97	0.96
Cl	4.22	1.62
Zn	2.94	0.61

(b)

Element	Wt%	Atomic%
C	68.65	78.89
O	19.57	16.88
Si	2.61	1.28
Cl	5.67	2.21
Zn	3.5	0.74

(c)

Element	Wt%	Atomic%
C	69.45	80.78
O	15.64	13.65
Si	3.65	1.81
Cl	7.46	2.94
Zn	3.81	0.81

(d)

Element	Wt%	Atomic%
C	67.19	80.80
O	13.78	12.44
Si	3.79	1.95
Cl	7.73	3.15
Zn	7.51	1.66

Fig. 5. EDS elemental composition of Si-QAC/ZnO/PDA@PET samples prepared with different zinc acetate concentrations: (a) 10 mmol·L^{-1}, (b) 20 mmol·L^{-1}, (c) 30 mmol·L^{-1}, and (d) 40 mmol·L^{-1}.

4.1.2.3. Chemical structure of the modified PET

ATR-FTIR spectra confirmed the presence of PET functional groups, PDA chemical bonds, immobilized ZnO NPs, and Si-QAC on the modified membrane surfaces (Fig. 6). Key PET characteristic peaks were consistently observed at 1710 cm^{-1} and 1245 cm^{-1}, corresponding to the C=O stretching in ester groups and the asymmetric C-C-O stretching linked to the aromatic ring, respectively [41]. Additionally, a broad peak near 1265 cm^{-1} was attributed to C-O stretching in PET ester groups [41]. Minor peaks at 1340 cm^{-1} and 1410 cm^{-1} represented trans and gauche CH_2 wagging bands, while peaks at 1470 cm^{-1} and 1100 cm^{-1} were associated with $-CH_2$ bending and C-O-C stretching vibrations, respectively [41]. New peaks emerged after modification, confirming successful functionalization. Peaks between 1600 cm^{-1} and 1650 cm^{-1}, exclusive to modified samples, were attributed to N-H bending vibrations of PDA groups, while broad peaks spanning 3000-3700 cm^{-1} corresponded to O-H and N-H vibrations of PDA nanospheres [32], [42]. Peaks in the 400-600 cm^{-1} range were linked to Zn-O stretching vibrations, indicative of ZnO NPs [43]. Although FTIR is primarily qualitative, the intensity variations in these peaks reflected differences in ZnO NP concentrations among the samples. Si-QAC incorporation was evident from distinct peaks at 2850 cm^{-1} and 2916 cm^{-1}, corresponding to C-H stretching bands characteristic of QAC groups [44]. These results confirm the successful modification of PET membranes with Si-QAC/ZnO/PDA, validating the presence of functional groups associated with each component.

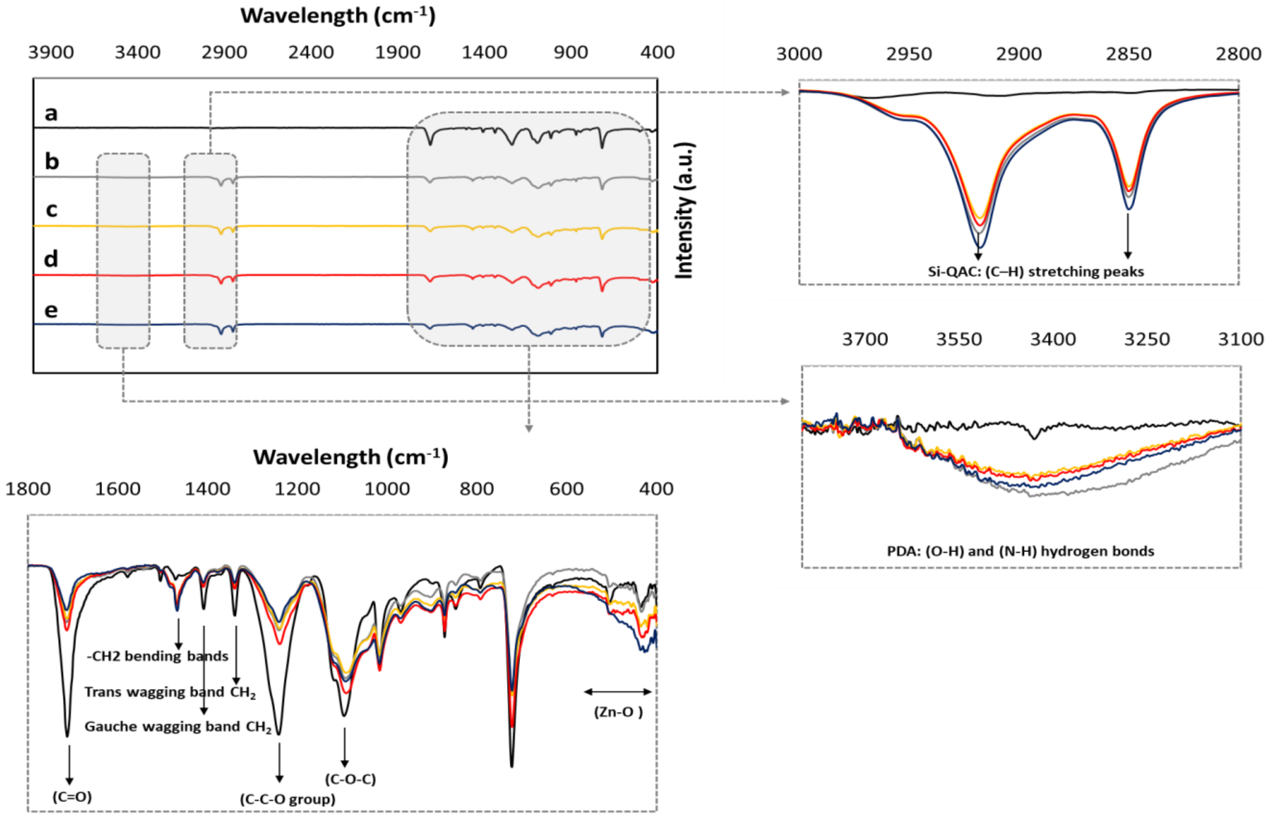

Fig. 6. ATR-FTIR spectra of blank PET (a, black) and Si-QAC/ZnO/PDA@PET membranes modified with varying zinc acetate concentrations: 10 mmol·L^{-1} (b, grey), 20 mmol· L^{-1} (c, yellow), 30 mmol· L^{-1} (d, red), and 40 mmol· L^{-1} (e, blue).

4.1.2.4. XRD, surface roughness and superhydrophobic properties

The XRD patterns of PET and PDA@PET samples showed no diffraction peaks corresponding to ZnO structures (Fig. 7a). However, ZnO-coated PDA@PET samples exhibited distinct peaks at 2θ values of 31.98°, 34.65°, 36.45°, 47.73°, 56.77°, 63.02°, 68.13°, and 69.22°, corresponding to the (100), (002), (101), (102), (110), (103), (112), and (201) planes of ZnO, respectively (Fig. 7a). The sharp diffraction peaks, particularly (100), (002), and (101), confirmed the crystalline nature and high purity of the ZnO NPs deposited on the surface, consistent with other studies [37], [45].

The surface roughness and profiles of pristine and surface-modified PET samples are presented in Fig. 7b. The pristine PET sample exhibited a root mean square (RMS) roughness of 2.07 nm, while the superhydrophobic PET sample showed a significantly higher roughness of 15.11 nm, over seven times greater. The pristine PET surface appeared smooth and uniform, whereas the superhydrophobic PET surface displayed a rough and textured morphology, attributed to hierarchical modifications (Fig. 7b). The size and density of nanoparticles are critical factors influencing surface roughness, as reported in previous studies [46], [47]. According to the Cassie-Baxter model, increased surface roughness enhances the WCA, contributing to greater hydrophobicity. Thus, the Si-QAC/ZnO/PDA@PET membrane's hydrophobicity was strongly affected by its surface roughness. Hierarchical nanocomposite modifications that increased roughness led to a higher WCA, thereby improving hydrophobicity.

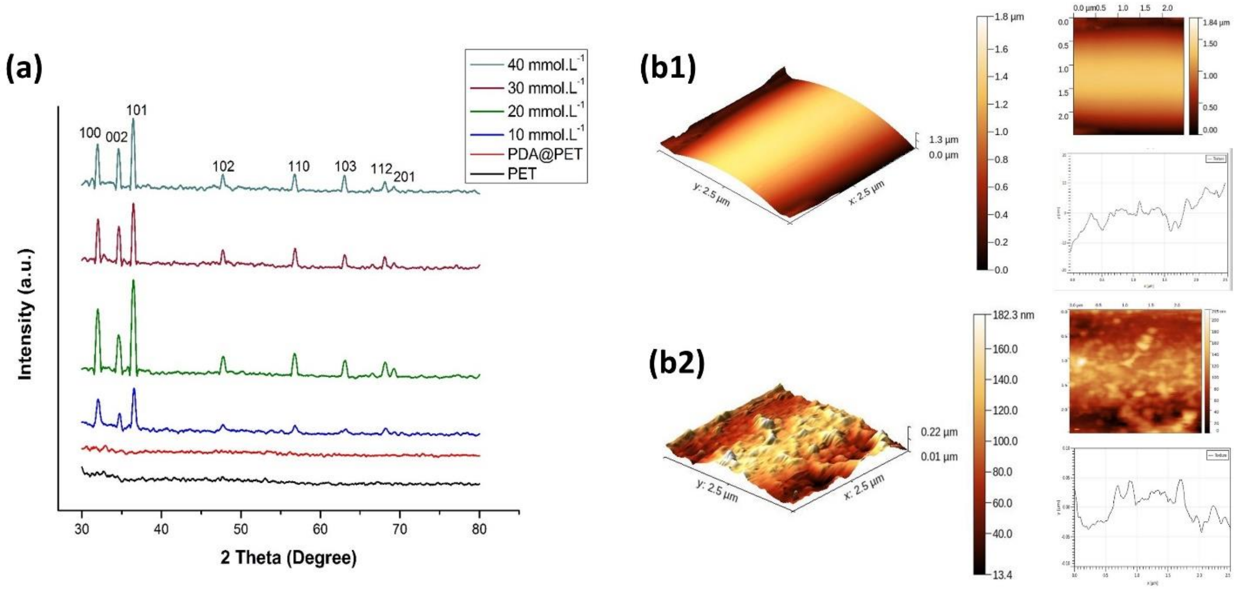

Fig. 7. (a) XRD patterns of the pristine and surface modified PET. (b) Surface roughness profiles of (b1) pristine PET and (b2) superhydrophobic Si-QAC/ZnO/PDA@PET sample.

To evaluate the role of ZnO NPs in achieving superhydrophobicity, PET samples were coated with Si-QAC alone, yielding a WCA of 130° and a roll-off angle of 19° (Fig. 8a). This hydrophobic surface lacked superhydrophobicity, as water droplets adhered strongly and did not roll off easily. Upon immobilizing ZnO NPs on the PET surface and subsequent Si-QAC silane treatment, the WCA increased beyond 150°, and the roll-off angle decreased to less than 6° (Fig. 8a), meeting superhydrophobic criteria [48], [49]. The superhydrophobic PET samples, modified with zinc acetate concentrations of 10, 20, 30, and 40 mmol·L^{-1}, exhibited WCAs of 152°, 157°, 157°, and 160° and roll-off angles of 6°, 5°, 4°, and 2°, respectively. The increase in WCA with higher zinc acetate concentrations correlated with greater surface roughness and denser ZnO NP distribution. These modifications formed micro/nanostructures with hierarchical arrangements, enhancing surface roughness and contributing to superhydrophobicity, as reported in similar studies [50], [51].

Superhydrophobicity in the modified PET samples aligns with the Cassie-Baxter model, where air trapped in surface cavities prevents water droplet penetration, forming a reflective plastron layer when submerged in water [52]. The hierarchical micro and nanostructures created air pockets, increasing air-liquid interfaces and enhancing hydrophobicity. These properties make the surfaces highly stable and suitable for applications requiring robust superhydrophobic performance [53], [54].

4.1.2.5. Stability of superhydrophobic properties

The stability of Si-QAC/ZnO/PDA@PET samples was assessed under various conditions, including cleaning, chemical exposure, mechanical abrasion, and UV radiation, as summarized in Fig. 8b. Despite a reduction in WCA after 20 cycles of sandpaper abrasion, all samples, regardless of zinc acetate concentration, maintained WCAs above 145°, preserving their hydrophobic properties. Notably, the sample prepared with 40 mmol·L^{-1} zinc acetate exhibited excellent abrasion resistance, retaining a WCA of 153° after mechanical abrasion. After five cleaning cycles, this sample retained the highest WCA of 156°, demonstrating its robustness and resistance to mechanical and frictional forces. The samples experienced a more significant decrease in WCA when exposed to alkaline solutions compared to acidic solutions, likely due to surface etching of the polyester fibers in the presence of alkaline conditions, according to the study [55]. However, all samples, regardless of zinc acetate concentration, showed no significant degradation under UV radiation. These results suggest that the Si-QAC/ZnO/PDA@PET samples exhibit promising long-term stability for practical applications.

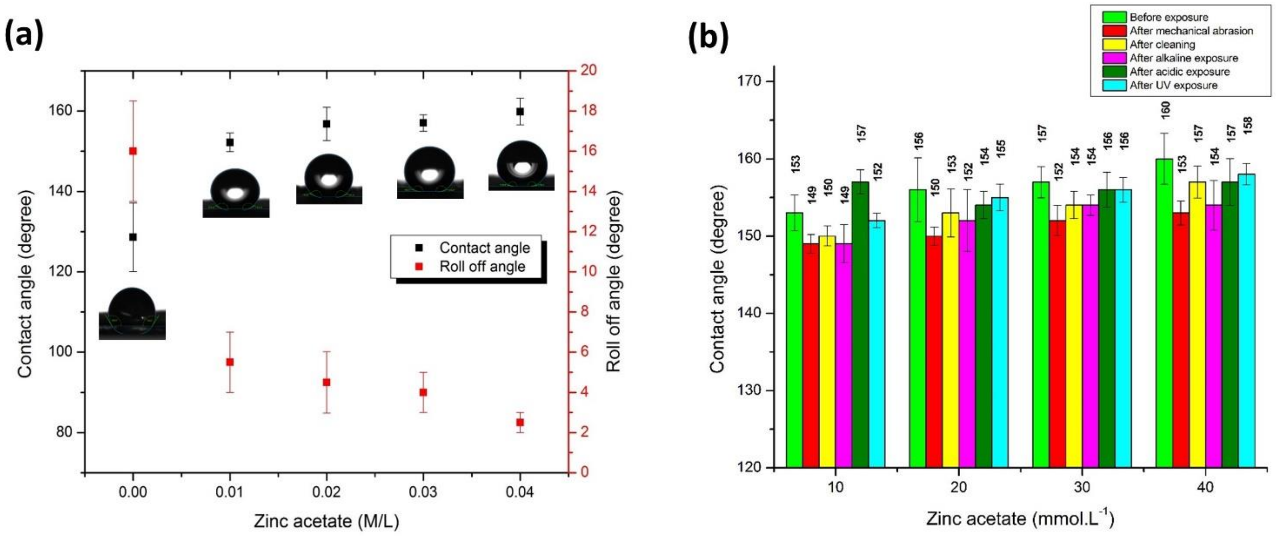

Fig. 8. (a) WCAs and roll-off angles of Si-QAC/ZnO/PDA@PET samples as a function of varying zinc acetate concentrations, and (b) changes in WCA illustrating the stability of Si-QAC/ZnO/PDA@PET samples with different zinc acetate concentrations under various environmental conditions.

4.1.2.6. Bacterial repulsive properties

As shown in Fig. 9, the pristine PET sample exhibited significant proliferation of *E. coli* and *Staphylococcus sp.*, indicating a high propensity for bacterial growth on the unmodified surface. In contrast, the Si-QAC/ZnO/PDA@PET samples demonstrated notable bacterial repulsion against both strains. These modifications reduced bacterial attraction and growth on the surface, showing a subtle but discernible repulsion near the contact zone. However, no significant differences were observed among the samples with varying ZnO NP concentrations. This can be attributed to the complete coverage of ZnO NPs by Si-QAC, which limited bacterial contact. Additionally, the strong immobilization of the nanocomposite coating prevented the release of ZnO NPs. The combined effects of Si-QAC coverage and the immobilization of the triple-layer structure contributed to the clear bacterial repulsive behavior.

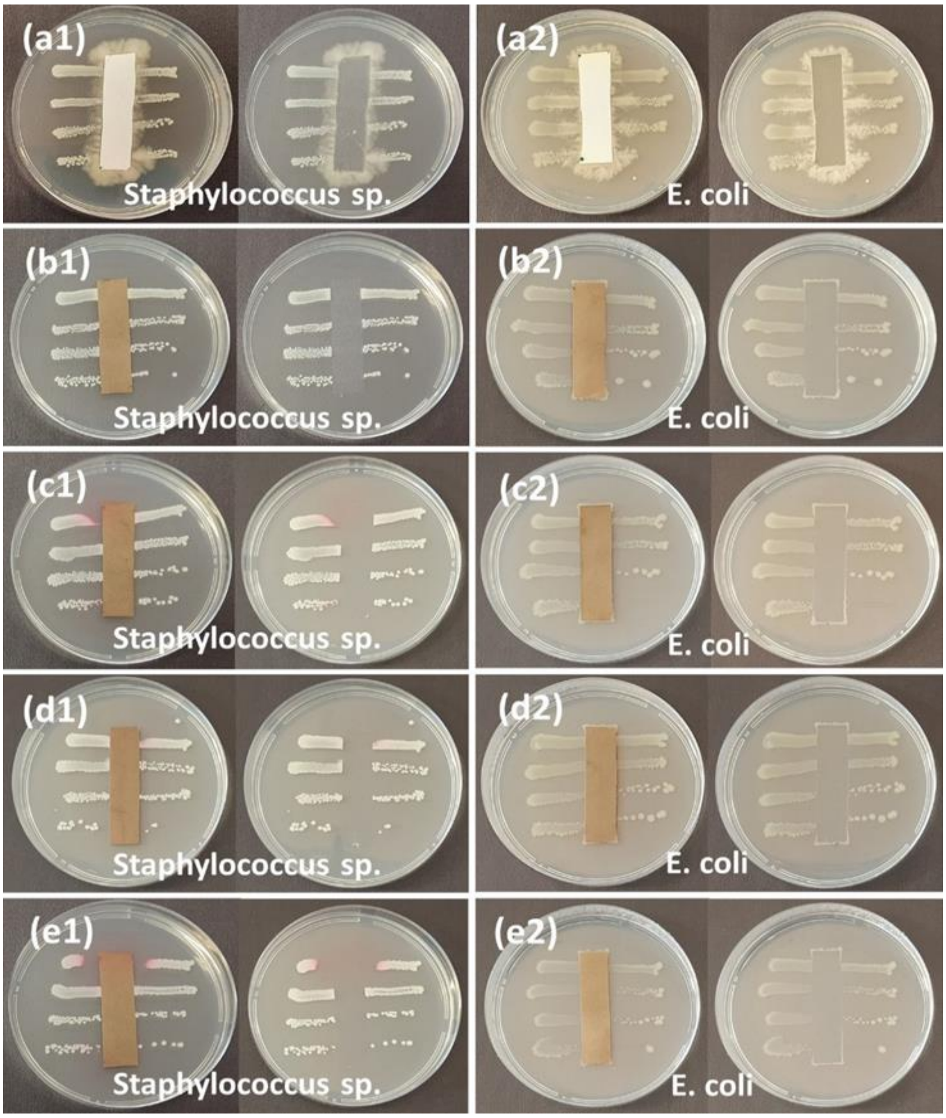

Fig. 9. Bacterial repulsive properties of blank and modified PET samples against different concentrations (10^0, 10^{-1}, 10^{-2}, and 10^{-3}) of (1) *Staphylococcus sp.* and (2) *E. coli* bacteria: (a) blank PET, and Si-QAC/ZnO/PDA@PET samples with varying zinc acetate concentrations: (b) 10 mmol·L^{-1}, (c) 20 mmol·L^{-1}, (d) 30 mmol·L^{-1}, and (e) 40 mmol·L^{-1}.

4.1.2.7. Physical self-cleaning and water-solvent separation properties

The physical self-cleaning capability of the Si-QAC/ZnO/PDA@PET samples is illustrated in Fig. 10a. Water droplets rapidly rolled off the superhydrophobic surface, effectively removing dyed micro-cellulose particles, mimicking the lotus effect due to the low surface energy and high liquid surface tension [56]. Time-lapse images (Fig. 10b) further show that water droplets bounced on the surface without being absorbed, highlighting the inherent superhydrophobicity of the Si-QAC/ZnO/PDA@PET sample.

Additionally, the Si-QAC/ZnO/PDA@PET samples acted as selective membranes, efficiently separating organic solvents from water. As shown in Fig. 11, the samples absorbed toluene and chloroform from water, leaving no visible traces of red oil, while the superhydrophobic surface retained a red coloration. This demonstrated the correlation between the superhydrophobicity induced by surface roughness and the incorporation of ZnO NPs in the membrane structure [57].

The water-solvent separation efficiency of Si-QAC/ZnO/PDA@PET membranes was evaluated by filtering a water mixture containing n-hexane, toluene, chloroform, and petroleum ether. The separation efficiencies were consistently over 93%, with specific values of 96%, 93%, 97%, and 94% for n-hexane, toluene, chloroform, and petroleum ether, respectively, indicating their suitability for such applications.

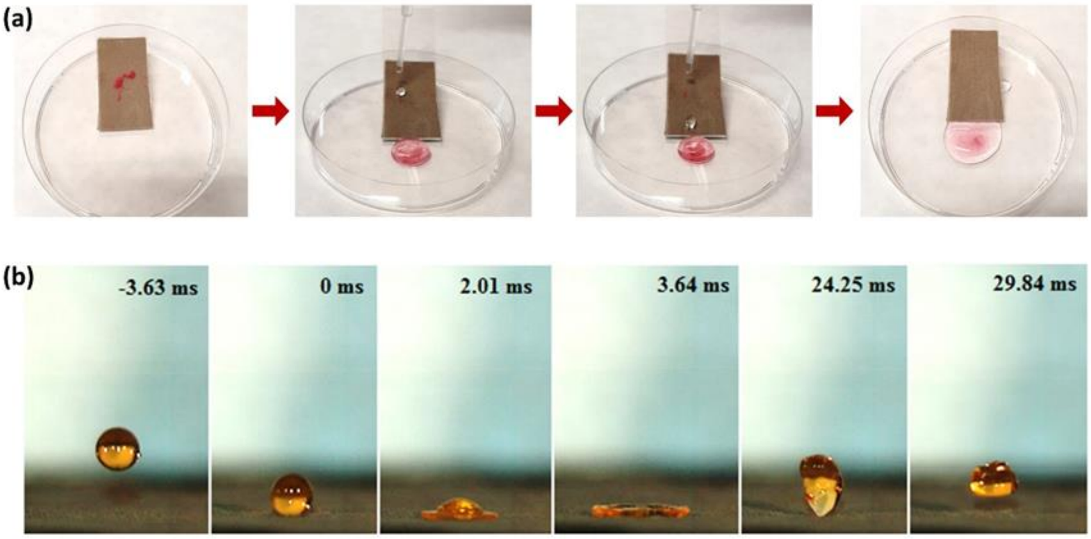

Fig. 10. Time course of (a) self-cleaning performance, and (b) bouncing of water droplet of Si-QAC/ZnO/PDA@PET sample.

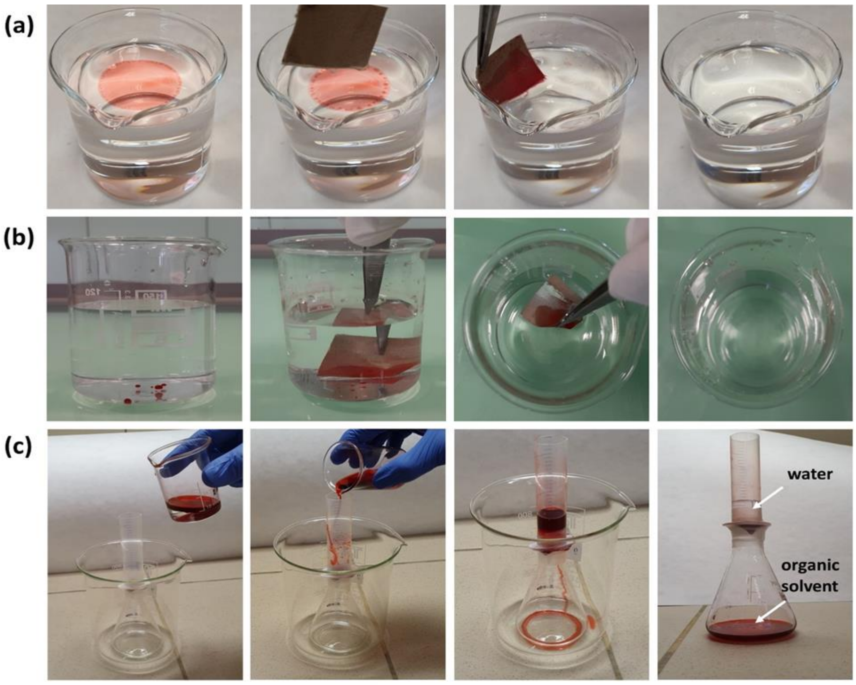

Fig. 11. Water-organic solvent separation experiment using Si-QAC/ZnO/PDA@PET membranes: (a) separation of toluene from water, (b) separation of chloroform from water, and (c) selective separation of toluene from water.

4.1.3. Summary

This study represents a significant advancement in the surface engineering of PET fabrics for efficient organic solvent-water separation. The innovative approach combines a hierarchical superhydrophobic nanocomposite coating with biomimetic PDA deposition, eco-friendly *in-situ* synthesis of ZnO NPs from sustainable sources, and non-fluorinated silane coverage. Analytical techniques, including SEM, EDS, FT-IR, and XRD, confirmed the successful modification of the PET surface with the Si-QAC/ZnO/PDA nanocomposite. The enhancement in surface roughness and hydrophobicity was evidenced by a WCA of 150°-160° and a roll-off angle of 2°-6°. The modified PET surface demonstrated effective bacterial repulsive properties, significantly reducing *E. coli* and *Staphylococcus sp.* adhesion. The robustness of the surface coating was confirmed under harsh conditions, including mechanical abrasion, repeated cleaning cycles, chemical exposure, and UV irradiation. These modifications yielded a high organic solvent-water separation efficiency, exceeding 90% across all tested solvents. This eco-friendly and sustainable surface modification method, utilizing the Si-QAC/ZnO/PDA nanocomposite, offers a durable solution for achieving long-term superhydrophobicity in PET fabrics, making it a promising technology for advanced separation applications.

4.2. Chapter 2: **Superhydrophilic surface modification**

4.2.1. Materials and method

4.2.1.1. Surface coating methodology

The oxidative polymerization of PDA on polytetrafluoroethylene (PTFE) HF (HF) membranes was performed using an air-stimulated method, relying on dissolved oxygen for auto-oxidation [58]. Identical lengths of PTFE HF membranes (Dongyang Hanchen Membrane Technology, China) were assembled into tubular modules, connected to an air compressor, and immersed in a reactive solution of 2 $mg{\cdot}mL^{-1}$ dopamine hydrochloride (Alfa Aesar, USA) in 10 $mmol{\cdot}L^{-1}$ TRIS buffer (pH 8.5) prepared with deionized (DI) water. The supplied air facilitated the oxidative polymerization of dopamine hydrochloride monomers, promoting the spontaneous growth of a PDA coating on PTFE HF MEMBRANEs. The reaction mixture was stirred for up to 28 hours, with the PDA layer thickening over time, indicated by a color change from colorless to black. Membranes were removed at selected intervals (4, 14, and 24 hours, as shown in Table 1) based on surface conversion characteristics, rinsed with DI water to eliminate unreacted agents, and subsequently soaked in DI water. In the second stage, ZnO NPs (Sigma-Aldrich, USA) were immobilized on PDA-coated HF membranes. ZnO NPs at varying concentrations (0.5-1.5 $mg{\cdot}mL^{-1}$) were dispersed in ethanol, ultrasonicated (Bandelin, Sonorex digitec, Germany; 35

kHz), and stabilized by zeta potential evaluation. A 2% v/v solution of (3-aminopropyl)triethoxysilane (APTES, TCI, USA) was added, and the mixture was vortexed and heated to 50 °C. The membranes were immersed in this solution for 1 hour, then rinsed thoroughly with DI water. Sample details with varying PDA and ZnO NPs concentrations are summarized in Table 1.

Table 1. Membranes' name and compositions.

Samples name	**Modification**	**PDA pol. time (h)**	**ZnO (mg.mL^{-1}) in Etanol**
Blank	Pristine PTFE HF MEMBRANE	0	0
PDA 4	PDA4@PTFE HF MEMBRANE	4	0
PDA 14	PDA14@PTFE HF MEMBRANE	14	0
PDA 24	PDA24@PTFE HF MEMBRANE	24	0
Sample 1	ZnO 0.5 & PDA 24@PTFE HF MEMBRANE	24	0.5
Sample 2	ZnO 1 & PDA 24@PTFE HF MEMBRANE	24	1
Sample 3	ZnO 1.5 & PDA 24@PTFE HF MEMBRANE	24	1.5

4.2.1.2. Characterizations

Morphological evaluations of surface-treated PTFE HF membranes were conducted using scanning electron microscopy (SEM, TESCAN ORSAY HOLDING a.s, Czechia), while energy-dispersive X-ray (EDX) analysis was used to determine surface elemental composition. Chemical bonds in the specimens were analyzed using Fourier-transform infrared (FT-IR) spectroscopy (Perkin Elmer Spectrum 65 FTIR, USA). Hydrophilicity changes in the modified PTFE HF membranes were assessed by WCA measurements. The dispersion of ZnO NPs in ethanol was evaluated using zeta potential measurements (Anton Paar), with triplicate tests for accuracy. Different ZnO NP concentrations were dispersed in ethanol, ultrasonicated for 30 minutes, and analyzed for zeta potential. Membrane porosity (%) was determined by measuring the weight difference between dry membranes and those saturated with isopropanol (IPA) [8], [59]. Both treated and pristine PTFE HF membranes were weighed dry (W_{dry}), immersed in IPA for 24 hours, drained vertically, and weighed wet (W_{wet}) after solvent evaporation. Porosity ($\mathcal{E}$) was calculated using equation (1) [8], [59].

The stability of ZnO NPs dispersed in ethanol was assessed for all samples by measuring the zeta potential in triplicate using a Zetasizer Nano Series (Malvern Instruments, UK). The modified coating's stability was further evaluated by quantifying the amount of ZnO NPs released from the membrane surface during filtration, using a modified leaching test [60], [61]. This was performed with a NexION 300D inductively coupled plasma-optical emission spectrometer (ICP-OES; PerkinElmer, USA), with a detection limit of 1.0 µg·L^{-1}. The leaching test involved filling a reservoir with 5 L of deionized (DI) water and fixing the modified HF membrane module in a dead-end filtration cell. Filtration was conducted at a transmembrane pressure (TMP) of 1.0 bar.

Permeate samples (10 mL) were collected at specific filtration volumes: 0.2 L (step 1), 0.5 L (step 2), 1.0 L (step 3), 1.5 L (step 4), 2.0 L (step 5), 2.5 L (step 6), 3.0 L (step 7), 3.5 L (step 8), 4.0 L (step 9), 4.5 L (step 10), and 5.0 L (step 11). To enhance detection accuracy, 0.2 mL of concentrated HNO_3 (14.58 mol·L^{-1}) was added to each permeate sample for ionization of Zn. After filtration, the membrane was removed, dried at 105 °C for 2 hours, and immersed overnight in 60 mL of concentrated HNO_3 (14.58 mol·L^{-1}) at room temperature to leach the remaining ZnO NPs. The concentrations of ZnO NPs in permeate and leachate samples (diluted 5×) were analyzed using ICP-OES. The stability of the ZnO NPs was calculated using equation (2).

$$\varepsilon\ (\%) = \frac{\left(\frac{W_{wet}-W_{dry}}{\rho_{IPA}}\right)}{\left(\frac{W_{wet}-W_{dry}}{\rho_{IPA}}\right)+\left(\frac{W_{dry}}{\rho_{PTFE}}\right)} * 100 \qquad (1)$$

$$Zn_r\ (\%) = \left(\frac{(Zn_r)_i}{\sum_{i=1}^{11}(Zn_r)_i + Zn_L}\right) * 100 \qquad (2)$$

, where ρIPA represents the density of IPA (0.78 g·cm^{-3}), and ρPTFE represents the density of PTFE (2.2 g·cm^{-3}). Zn_r represents the amount of ZnO nanoparticles released during each water filtration interval, while Zn_L denotes the ZnO NPs leached from the membrane surface.

4.2.1.3. Flux recovery of membranes

A dead-end cell connected to an air compressor (with TMP regulated by an airflow meter) and a DI water supply tank was used to assess the flux recovery of PTFE HF membranes before and after modification. Filtration experiments were conducted at room temperature. HF membranes modules were fixed in the cell, equilibrated for 30 minutes at 1.0 bar TMP, and operated for 1 hour. The flux at each filtration step, initial water flux (J_1), bovine serum albumin (BSA) flux (J_{BSA}), and secondary water flux (J_2), was calculated using Equation (3) [9], [21], [62]. The membrane rejection ratio (RR) was determined using Equation (4) after 1 hour of BSA filtration (1.0 mg·mL^{-1}) [21], [63], [64]. Following BSA filtration, the HF membranes were removed, washed with DI water, reinstalled, and tested for secondary water flux (J_2) over 1 hour to calculate flux recovery after protein filtration. Anti-fouling performance was evaluated using the flux recovery ratio (FRR) via Equation (5) [59], [62], while total membrane fouling (R_{total}) was calculated using Equation (6) [59], [65]. Reversible fouling (R_{rev}), caused by removable foulants, was determined with Equation (7) [59], [65]. Irreversible fouling (R_{irr}), representing non-removable deposits, was calculated using Equation (8) [59], [65].

$$J_1 = \frac{V}{(\Delta t * A)} \qquad (3)$$

$$RR\ (\%) = \left(1 - \frac{C_{permeate}}{C_{feed}}\right) * 100 \qquad (4)$$

$$FRR\ (\%) = \left(\frac{J_2}{J_1}\right) * 100 \qquad (5)$$

$$R_{total}(\%) = \left(1 - \frac{J_{BSA}}{J_1}\right) * 100 \quad (6)$$

$$R_{rev}(\%) = \left(\frac{J_2 - J_{BSA}}{J_1}\right) * 100 \quad (7)$$

$$R_{irr}(\%) = \left(\frac{J_1 - J_2}{J_1}\right) * 100 \quad (8)$$

, where V is the permeate volume (L), A is the membrane surface area (cm^2), Δt is filtration process time (h), $C_{permeate}$ and C_{feed} are permeated, and initial BSA concentration, which can be measured by the UV – vis spectroscopy analysis, respectively.

4.2.1.4. Antimicrobial evaluation

The antimicrobial effects of surface-modified PTFE HF membranes with varying amounts of immobilized ZnO NPs (samples 1, 2, and 3 according to Table 1) was quantitatively compared under dynamic contact conditions using the ASTM E2149 standard. *Staphylococcus sp.* (Gram-positive) and *E. coli* (Gram-negative) were used as test bacteria [66], [67]. The dynamic contact method ensures full contact between test specimens and bacterial inoculum, enabling accurate quantitative comparison based on specific contact times. Bacterial strains *Staphylococcus sp.* (CCM 2446) and *E. coli* (CCM 7395) were obtained from the Czech Collection of Microorganisms (*Brno, Czech Republic*). Colony-forming units (CFUs) were evaluated using cultivation techniques, with bacterial stocks prepared to an exponential growth phase (1×10^5 cells in 1 mL). The bacterial cultures were diluted 10, and 100-fold in 0.85% NaCl and prepared for antimicrobial testing on Plate Count Agar (PCA, Bio-Rad, France). Analyses were performed in duplicate at 0 and 24 hours, with CFUs measured at 0, 1, 3, 6, and 24 hours to assess antimicrobial performance. For testing, 0.5 g of membrane was immersed in 25 mL of bacterial medium and incubated at 120 rpm. Samples (1 mL) were taken at 0, 1, 3, 6, and 24 hours, seeded onto PCA plates, and incubated at 37 °C for 48 hours. The CFUs were quantified in $\log_{10}$ ($CFU \cdot mL^{-1}$). The reduction value (RV) and reduction percentage (R%) of pristine and modified PTFE HF membranes were calculated using equations (9) and (10) [68], [69].

$$R_V = \log_{10}(B)_{contact\ time} - \log_{10}(A)_{contact\ time} \quad (9)$$

$$R_{\%} = \left(\frac{B-A}{B}\right) * 100 \quad (10)$$

, where B and A are CFU of the blank and surface-modified membranes, respectively.

4.2.2. Results and discussion

4.2.2.1. ZnO NPs' zeta potential

Table 3 presents the zeta potential of samples with varying ZnO content. A 0.5 $mg \cdot mL^{-1}$ ZnO NP/EtOH solution (Sample 1) exhibited an average zeta potential of 17.97 mV, indicating poor dispersion. In contrast, solutions with 1.0 $mg \cdot mL^{-1}$ (Sample 2) and 1.5 $mg \cdot mL^{-1}$ (Sample 3) showed average zeta potentials of 35.03 mV and 32.2 mV, respectively (Table 2). Since zeta potentials of ±28 mV or higher are generally considered indicative of stable dispersion [70], [71], the 1.0 mg·mL^{-1} ZnO NP/EtOH solution appears sufficiently dispersed for immobilization onto membrane surfaces.

Table 2. Zeta potential of different ZnO NP concentrations dispersed in ethanol.

Sample	Repeat	ZnO (mg·mL^{-1})	Zeta Potential (mV)	Ave. ZP (mV)	SD (mV)
sample 1	1	0.5	18.8	17.97	1.1
	2		16.7		
	3		18.4		
sample 2	1	1	38.7	35.03	4.0
	2		35.6		
	3		30.8		
sample 3	1	1.5	33.6	32.20	1.2
	2		31.2		
	3		31.8		

4.2.2.2. Membrane surface characterization

SEM analysis illustrated the incremental growth of PDA on PTFE HF membranes surfaces at 4, 14, and 24 hours of polymerization. At higher magnification (20kx, Fig. 12, a2-d2), a 24-hour polymerization time resulted in uniform and homogeneous surface coverage. However, at lower magnification (2kx, Fig. 12, a1-d1), no significant differences were observed, indicating the minimal impact of PDA growth on the porous surface morphology. The SEM images also highlighted the role of air stimulation in PDA growth. Without aeration, PDA showed poor and clumped growth on the PTFE surface (Fig. 13 a, b). Additionally, SEM analysis revealed that PDA alone was insufficient for robust immobilization of ZnO NPs, as most NPs were washed away during DI water rinsing (Fig. 13 c). However, the use of APTES as a crosslinker reversed this issue, enabling effective immobilization of ZnO NPs on PDA-treated PTFE HF membranes (Fig. 13 d). EDX analysis confirmed the minimal Zn immobilization by PDA alone but showed significantly higher Zn retention on APTES-treated membranes. The Zn immobilization increased proportionally with higher ZnO NP concentrations in the reaction mixture (Samples 1, 2, 3), as detailed in Table 3.

FT-IR analysis confirmed the presence of PDA functional groups and silane-mediated ZnO immobilization on the PTFE HF membrane surfaces. ATR-FTIR spectra before and after surface modification (Fig. 14) displayed two peaks at ~1140 cm^{-1} and ~1200 cm^{-1}, corresponding to the stretching vibrations of C-F bonds [72], [73]. In PDA-coated PTFE HF membranes, new peaks emerged between 1300–1700 cm^{-1}, attributed to C-H, N-H, and O-H covalent bonds, and between 2400-3600 cm^{-1}, representing O-H and N-H hydrogen bonds [42], [62], [64]. A peak at 1605 cm^{-1} in the 24-hour PDA-modified sample, associated with amine N-H bond deformation, shifted to 1570 cm^{-1} in samples with crosslinked ZnO NPs [42]. Additionally, a broad peak around 1010 cm^{-1}, attributed to Si-O bond vibrations, appeared exclusively in samples containing

ZnO NPs, indicating the presence of APTES [74]. These findings confirm the successful modification of PTFE HF membranes with PDA and silane-mediated ZnO NPs.

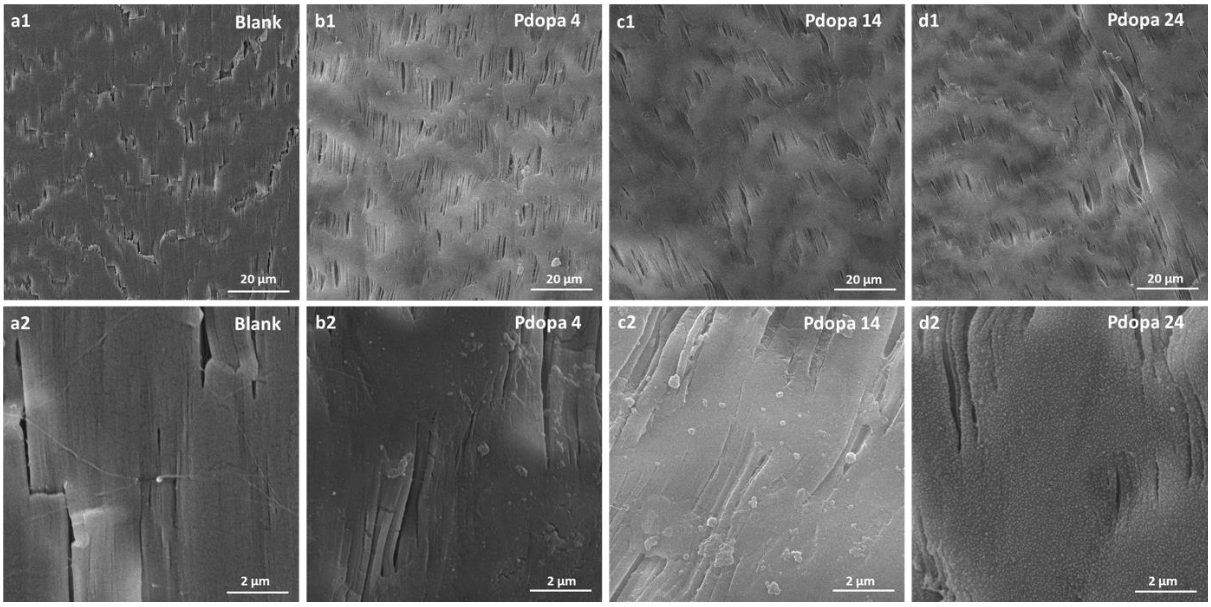

Fig. 12. SEM images of PDA-modified PTFE HF membranes at different polymerization times and magnifications {2 kx= a1-d1 & 20 kx= a2-d2 }:

a) Pristine PTFE (blank), b) PDA4@PTFE (4 h), c) PDA14@PTFE (14 h), and d) PDA24@PTFE HF membrane (24 h).

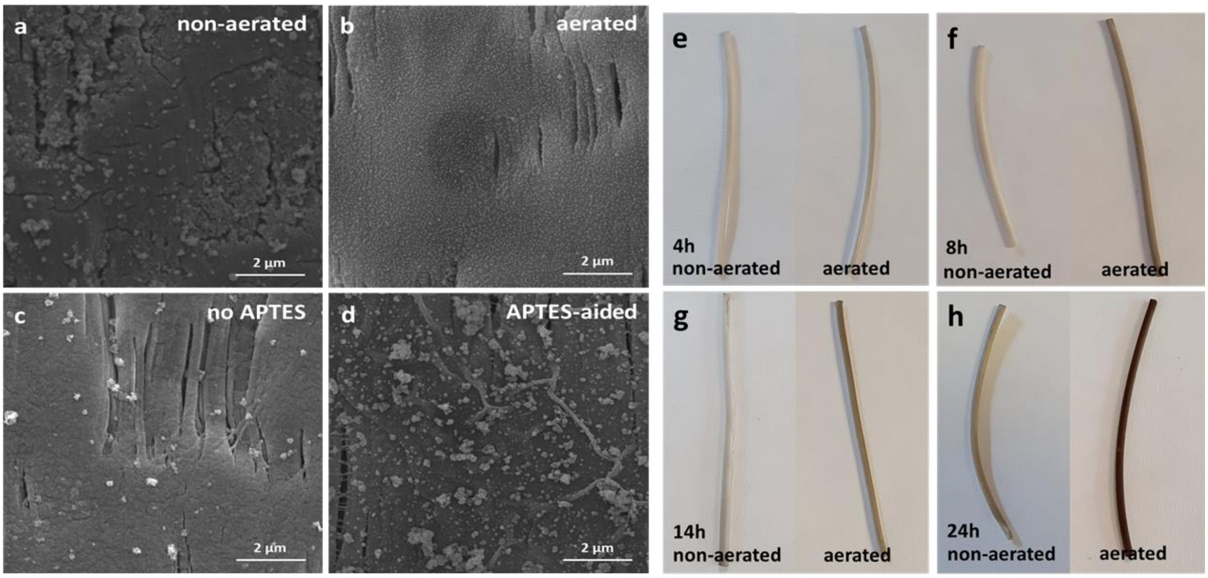

Fig. 13. SEM images and photographs of comparisons between different procedures: a) non-aerated, b) aerated PDA polymerization, c) no APTES, and d) APTES-aided ZnO NP immobilization on PTFE HF membrane. Photographs (e – h).

Table 3. Energy-dispersive X-ray surface elemental analysis of samples 1 to 3.

	C		N		O		F		Si		Zn		Total
	Wt. (%)	At. (%)	Wt. (%)	At. (%)	Wt. (%)	At. (%)	Wt. (%)	At. (%)	Wt. (%)	At. (%)	Wt. (%)	At. (%)	
Sample 1	25.29	35.12	1.46	1.74	3.84	4.00	65.17	57.21	2.51	1.49	1.72	0.44	100.00
Sample 2	24.88	36.08	0.69	0.86	3.55	3.86	61.46	56.35	0.98	0.61	8.44	2.25	100.00
Sample 3	23.68	36.89	1.46	1.95	7.23	8.45	46.58	45.88	2.10	1.40	18.95	5.43	100.00

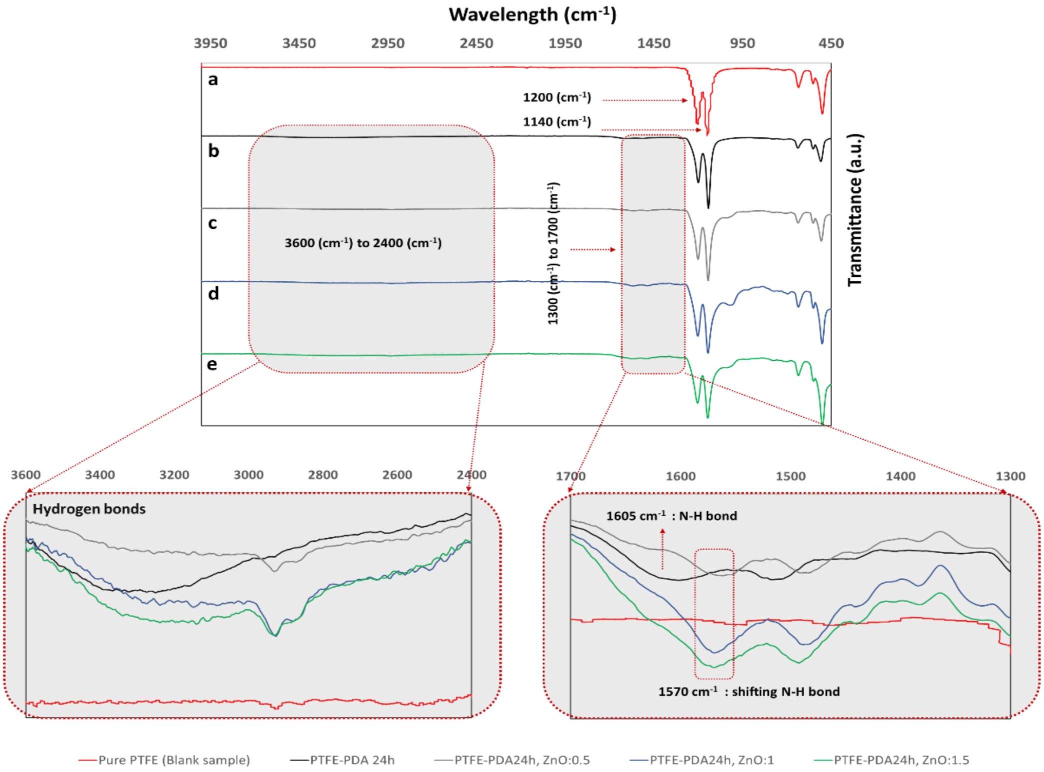

Fig. 14. FT-IR analysis of a) Pristine PTFE (Blank), b) PDA24@PTFE, c) Sample 1 (ZnO 0.5 & PDA 24@PTFE), d) Sample 2 (ZnO 1 & PDA 24@PTFE), and e) Sample 3 (ZnO 1.5 & PDA 24@PTFE) membranes.

4.2.2.3. WCA, porosity and ZnO NPs stability

The WCA test demonstrated that PDA modification significantly enhanced the hydrophilicity of PTFE HF membranes, with the WCA decreasing from 131° to 0° after 24 hours of aerated polymerization (Fig. 15a). The increased hydrophilicity resulted from the attachment of polar groups to the PTFE surface, rendering it superhydrophilic. These findings align with SEM images (Fig. 12d, Fig. 13d), which confirmed uniform surface coverage after 24 hours of PDA treatment. Immobilization of ZnO NPs using 2% v/v APTES for 1 hour, followed by washing, did not compromise the hydrophilicity of the modified membrane. Consistent with water flux and WCA results, extended PDA deposition slightly reduced membrane porosity from 54% to 45% due to pore constriction by the growing PDA layer (Fig. 15a) [13], [75]. A key advantage of the PDA modification technique is its ability to adhere to and grow on the surface/substrate rather than within the pores [76]. This feature prevents complete pore blockage, unlike other coating methods. Additionally, incorporating ZnO NPs onto the membrane surface had no significant effect on porosity, which remained around 45%.

ICP-OES analysis showed that during the initial filtration of 200 mL DI water, 97.41 µg·L^{-1} of Zn was released from the membrane surface into the permeate (Fig. 15b). Over time, the Zn release stabilized at approximately 40.00 µg·L^{-1}. This corresponds to less than 0.5 wt% of the total immobilized ZnO NPs (38721.43 µg·L^{-1}), confirming the stability of the ZnO NPs on the PTFE HF membrane surface. Furthermore, the stability evaluation was conducted at a higher TMP (1.0 bar) compared to the standard operating pressure for these membranes, typically ≤0.3 bar, underscoring the robustness of the modified coating.

4.2.2.4. Membrane flux recovery

The surface-modified membranes were evaluated against pristine membranes for their ability to recover initial flux after BSA filtration. Initial water fluxes (J_1) for uncoated PTFE HF membranes, PDA-coated PTFE HF membranes, and membranes modified with ZnO NPs were 307, 97.2, and 81.7 L·m^{-2}·h^{-1}, respectively (Fig. 15c). The reduced flux of PDA-coated membranes was attributed to PDA layer growth, which affected pore size and porosity. During BSA filtration, fluxes were lower for all membranes due to BSA adsorption and deposition, consistent with previous studies [11], [65] (Fig. 15d).

The flux recovery ratio (FRR) reflects a membrane's ability to regain its initial flux after filtration and cleaning cycles. Higher FRR values indicate better performance recovery and anti-fouling properties, reducing susceptibility to fouling caused by particles, proteins, or pollutants that block pores and reduce flux. Membranes with high anti-fouling characteristics allow easier removal of fouling layers and improved flux recovery after cleaning. FRR values for PDA-modified and ZnO NP-incorporated membranes were 76% and 68%, respectively, compared to only 29% for pristine membranes (Fig. 15d). The low FRR for pristine membranes was attributed to severe fouling from BSA deposition. PDA surface polymerization significantly improved flux recovery by discouraging BSA attachment, enhancing hydrophilicity, and facilitating protein removal, consistent with earlier findings [11], [77], [78].

Secondary flux (J_2) was consistently lower than J_1 due to residual fouling. Total membrane fouling (R_{total}), comprising reversible (R_{rev}) and irreversible (R_{irr}) fouling [59], was highest for pristine membranes (81.9%) compared to PDA-modified (64.6%) and ZnO-incorporated membranes (49.3%). Modified membranes showed improved anti-fouling properties by reducing irreversible fouling and enhancing the proportion of reversible fouling. The rejection ratio also improved from 66.0% for pristine membranes to 85.3% for PDA-modified membranes and 79.8% for ZnO-incorporated membranes (Fig. 15d). PDA modification created a hydrophilic barrier that minimized protein attachment and facilitated BSA removal during cleaning [65]. Although PDA-modified membranes showed better anti-fouling properties than ZnO NP-incorporated ones, both demonstrated significant FRR improvement over pristine membranes, confirming enhanced anti-fouling capabilities.

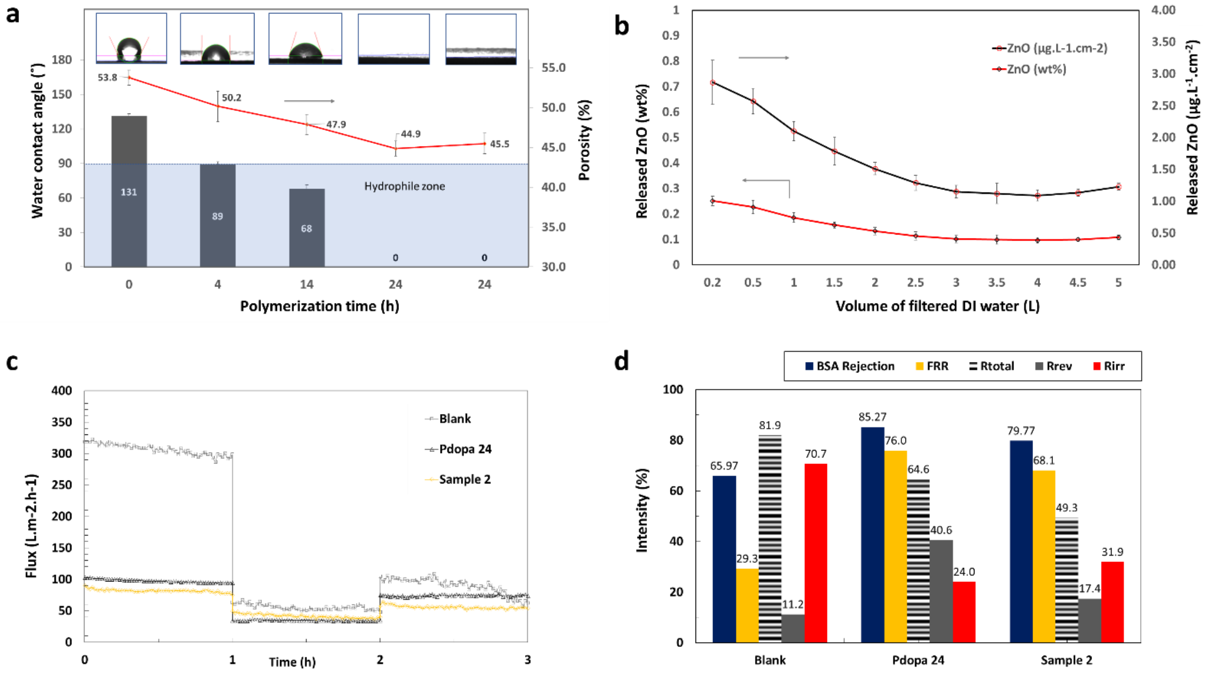

Fig. 15. a) WCA and porosity measurements; b) Leaching stability analysis of immobilized ZnO NPs released during the filtration procedure; c) Membrane flux recovery diagrams; and d) rejection, FRR, R_{total}, R_{rev}, and R_{irr} values.

4.2.2.5. Antimicrobial properties

Evaluation of colony-forming units (CFUs) revealed no antibacterial activity for pristine PTFE HF membranes against *Staphylococcus sp.* or *E. coli*, highlighting their susceptibility to biofouling in bioreactors (Figs. 16 a,b). Contrary to earlier studies suggesting PDA's antibacterial properties [79], [80], the PDA-modified membranes in this study exhibited no significant antimicrobial activity against either bacterial strain (Figs. 16 a,b). However, additional modification with ZnO NPs, a widely used less toxic antimicrobial agent [81], [82], significantly improved the membranes' resistance to bacterial growth (Samples 1, 2, 3; Table 1).

Microbial assessments showed that all ZnO NP-modified membranes exhibited immediate antimicrobial activity upon bacterial inoculation (Figs. 17 a,d). Membranes with higher ZnO NP concentrations (Samples 2 and 3) achieved 100% bacterial reduction within 6 h and 3 h against *E. coli* and *Staphylococcus sp.*, respectively. In comparison, Sample 1 (0.5 mg·mL^{-1} ZnO NPs) required 24 h to achieve similar reductions, 99% for *E. coli* and 100% for *Staphylococcus sp.* (Figs. 17 b,e). Reduction values > 2, indicating effective antimicrobial activity [83], were achieved by Samples 2 and 3 within 6 h and 3 h for *E. coli* and *Staphylococcus sp.*, respectively (Figs. 17 c,f). Sample 1 also showed antimicrobial effectiveness but only after 24 h of contact. After 24 h, all ZnO NP-modified samples (1, 2, and 3) achieved bacterial reduction values of 4.53 for *E. coli* and 4.36 for *Staphylococcus sp.*. In contrast, PDA-modified membranes exhibited minimal antimicrobial activity, with reduction values after 24 h contact reaching only 0.74 for *E. coli* and 0.1 for *Staphylococcus sp.*, confirming their limited effectiveness against bacterial growth. This highlights the critical role of ZnO NPs in enhancing the antibacterial performance of modified PTFE HF membranes.

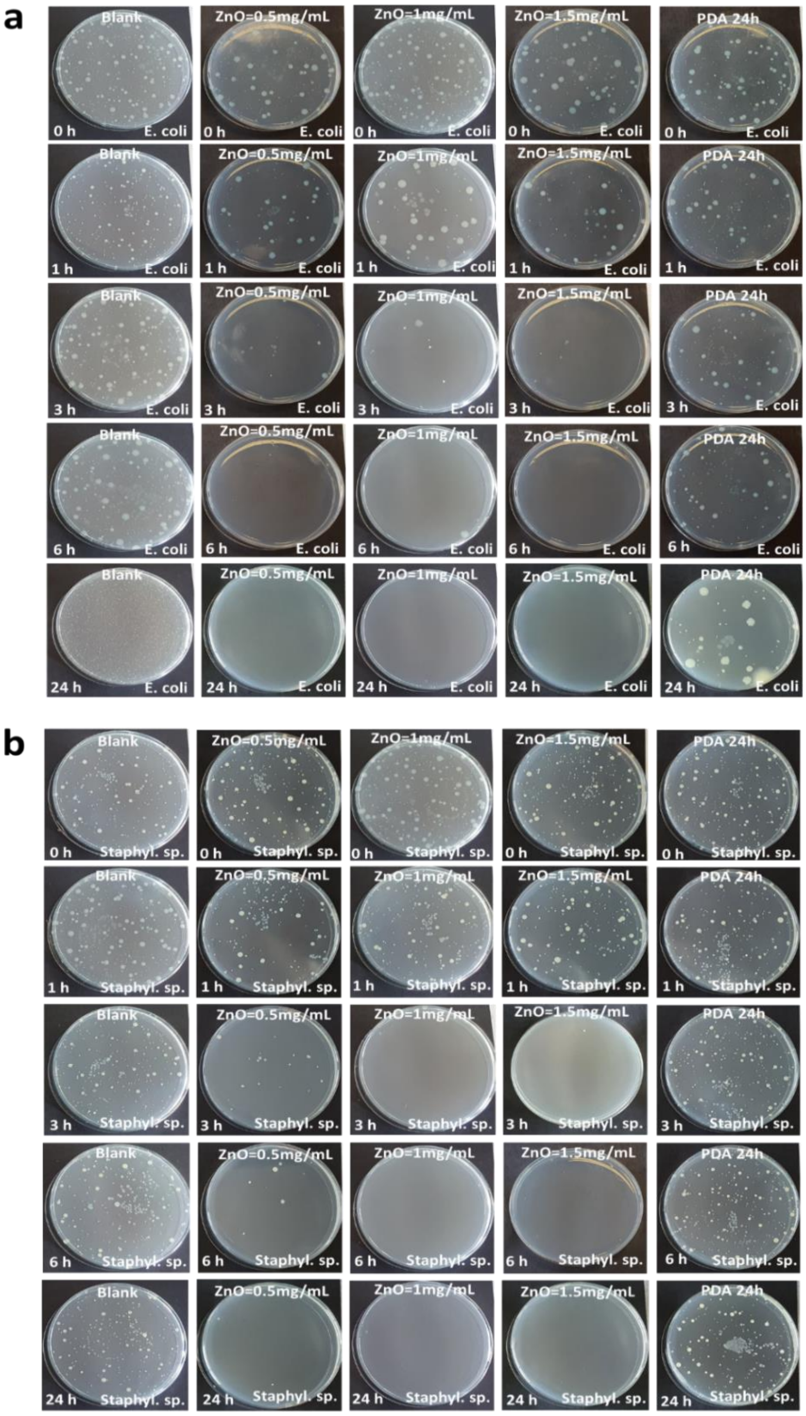

Fig. 16. Dynamic antimicrobial analysis activity against: a) *E. coli*, and b) *Staphylococcus* sp.

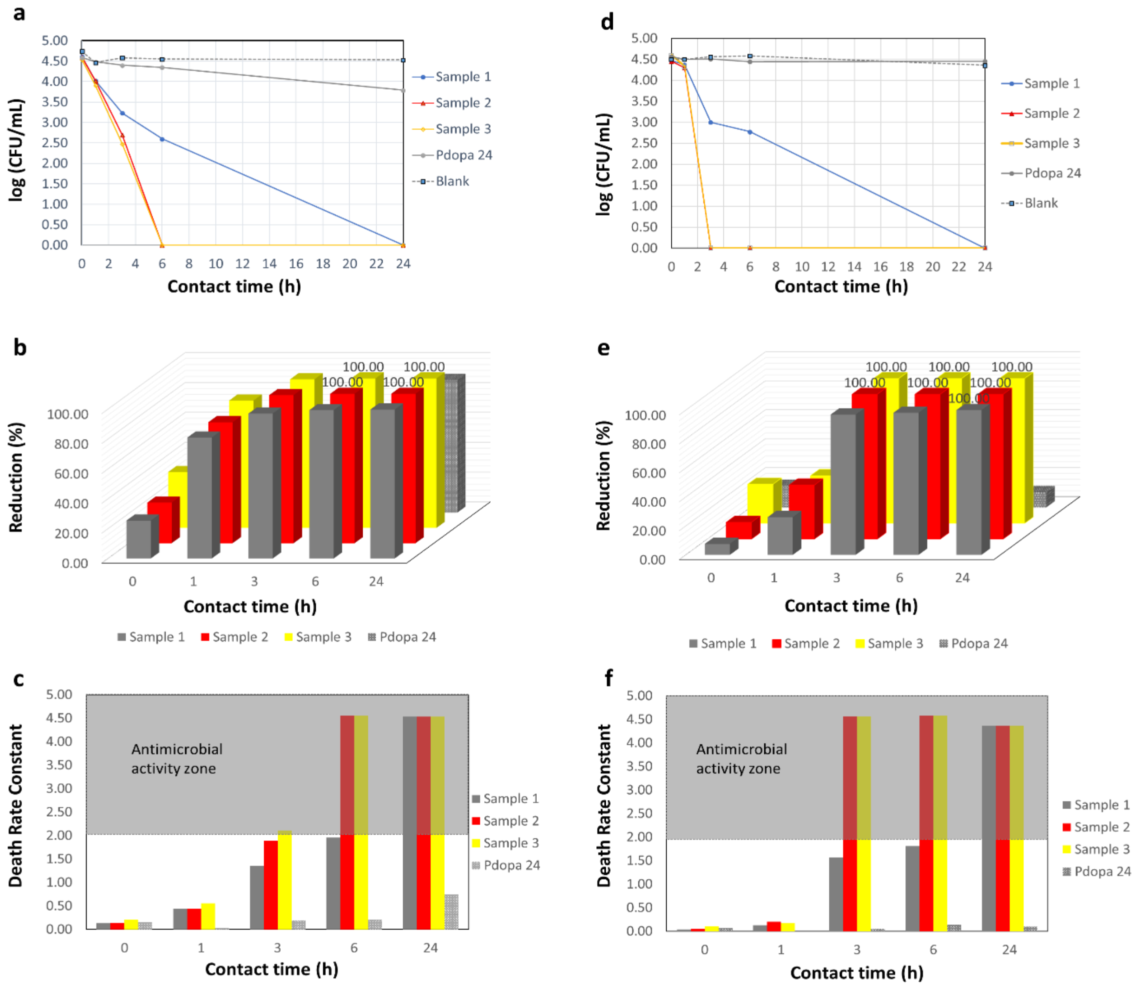

Fig. 17. Antimicrobial activity of pristine and surface-modified PTFE HF membranes: total number of CFU (logarithmic scale) against a) *E. coli* and d) *Staphylococcus* sp.; reduction value (RV) against b) *E. coli* and e) *Staphylococcus* sp.; and reduction percentage (R%) against c) *E. coli* and f) *Staphylococcus* sp.

4.2.3. Summary

In this study, an air-stimulated surface modification technique was employed to enhance the properties of PTFE HF membranes through the polymerization of PDA and incorporation of ZnO NPs. The optimized coating, featuring excellent properties, was achieved via 24 hours of air-stimulated polymerization of PDA and subsequent immobilization of ZnO NPs using APTES in ethanol. Morphological characterization revealed that the diffused air significantly accelerated the homogeneous growth of the PDA layer on the PTFE surface. The successful transformation of the PTFE HF membrane surface to a superhydrophilic state was confirmed by WCA measurements. FT-IR and EDX analyses verified the presence of PDA and ZnO on the membrane surface, while ICP analysis demonstrated the stability of the modified coating during operation. Functional improvements were validated through protein filtration and antimicrobial activity assessments. The flux recovery rates increased to 76% after PDA coating and 68% after ZnO NP immobilization, while fouling tendencies decreased to 64.6% and 49.3%, respectively, compared to 81.9% for unmodified membranes. Furthermore, the modified membranes achieved 100% bacterial reduction against *E. coli* and *Staphylococcus sp.* within short inoculation times of 6 hours and 3 hours, respectively, highlighting their superior anti-biofouling performance. The consistent results from experimental characterizations and functional analyses confirm the reliability of this novel approach. This study introduces a practical and sustainable air-stimulated method for creating superhydrophilic, fouling-resistant PTFE HF membranes using PDA and ZnO NPs, with significant potential for applications in advanced water treatment systems.

4.3. Chapter 3: **Fouling rate and critical flux evaluation of the modified membranes**

4.3.1. Materials and method

4.3.1.1. Dual-step surface modification and characterization

The PES HF membrane underwent surface modification following a two-step process. Initially, PDA surface polymerization was carried out by immersing PES HF membrane modules (Shandong Jinhuimo Technology Co., China) in a 10 $mmol \cdot L^{-1}$ Tris(hydroxymethyl)aminomethane (Penta, Czechia) buffer solution. Dopamine hydrochloride (Alfa Aesar, USA) was polymerized at a pre-adjusted pH of 8.5 for durations of 1.0, 2.5, and 4.0 hours, respectively. The membranes were then rinsed three times with deionized (DI) water to remove any unreacted monomers. In the subsequent step, the PDA-coated PES HF membranes were immersed in a ZnO seed solution prepared by dissolving zinc acetate in DI water (0.02 $mol \cdot L^{-1}$). The in-situ synthesis and immobilization of ZnO NPs were achieved by vigorously stirring the solution at 80°C while gradually adding 2.0 $mol \cdot L^{-1}$ Tris buffer to adjust the pH to 9. The membrane modules remained in the solution for an additional hour. Finally, the PDA-coated PES HF membranes with immobilized ZnO NPs were thoroughly rinsed with DI water to remove any unattached particles and stored in DI water for subsequent experiments.

The surface morphology of the modified PES HF membrane was characterized by field emission scanning electron microscopy (FE-SEM, Zeiss, Germany) to visually assess the modifications. Energy-dispersive X-ray spectroscopy (EDX) was utilized to analyze the elemental composition of the exterior surface after modification and generate high-contrast elemental distribution images.

4.3.1.2. Filtration and fouling rate measurement

The permeabilities of both pristine and surface-modified membranes were evaluated by gradually increasing the flux and collecting permeate while monitoring the TMP at 4-minute intervals. Each test was conducted three times, and the slope of the regression line from the flux versus TMP data was used to determine the membrane's permeability. The fouling rate (FR) represents the instantaneous rate of TMP increase over time, as expressed in equation (11) [15]:

$$FR = \frac{dTMP}{dt} \tag{11}$$

The critical flux is defined as the flux beyond which the rate of change of TMP over time exhibits a sudden increase. Typically, this corresponds to a fouling rate exceeding the threshold of 0.5 $\text{mbar}\cdot\text{min}^{-1}$, marking the onset of significant membrane fouling [16]. The critical flux of the membranes was determined using a flux-step experiment, as described in [15]. The flux-step method with 10-minute intervals per cycle began with flux steps of approximately 13 ($\text{L}\cdot\text{m}^{-2}\cdot\text{h}^{-1}$) and gradually increased to a maximum of about 40 ($\text{L}\cdot\text{m}^{-2}\cdot\text{h}^{-1}$). Each flux step was repeated, resulting in a total permeate collection time of 20 minutes per step.

4.3.1.3. Antimicrobial assessment

The antimicrobial activity of the surface-modified PES HF membranes containing ZnO NPs was evaluated under dynamic contact conditions similar to the mentioned method in section 4.2.1.4, in accordance with ASTM E2149 standard [84]. Bacterial cultures, including Gram-positive *Staphylococcus sp.* CCM 2446 and Gram-negative *E. coli* CCM 7395 (obtained from the Czech Collection of Microorganisms, Brno, Czechia), were grown to the mid-logarithmic growth phase (approximately 1×10^5 cells in 1 mL). Membrane samples weighing 0.5 g were immersed in 25 mL of the bacterial culture and homogenized at 120 rpm. At specific time intervals (0, 2, 5, and 24 hours), 1.0 mL of the solution was extracted and pipetted onto Plate Count Agar (PCA, Bio-Rad, France). The samples were serially diluted (10-fold and 100-fold) to achieve final dilutions of up to 10^4 and 10^3 cells in 1 mL, using a sterile physiological saline solution (8.5 $\text{g}\cdot\text{L}^{-1}$ NaCl in DI water). The plates were incubated at 37°C for 48 hours, after which the CFUs were quantified. The bacterial CFU counts were expressed on a $\log_{10}$ scale ($\text{CFU}\cdot\text{mL}^{-1}$) for comparison.

4.3.2. Results and discussion

4.3.2.1. Membrane surface characterization

SEM images of the PES HF membranes, before and after surface modification, revealed that the growth of the PDA nanolayer is time-dependent. As the polymerization time increased to 1.0, 2.5, and 4.0 hours, the PDA nanospheres showed progressively greater surface coverage (Fig. 18). This growth correlated with a reduction in both the pore size and porosity of the PES membrane. Additionally, SEM images captured using a high-contrast lens offered enhanced clarity, enabling more detailed visualization of the immobilized ZnO nanoparticles (NPs) and PDA nanospheres on the membrane surface (Fig. 18e). EDX elemental composition data confirmed the successful immobilization of ZnO NPs. The uniform and non-agglomerated dispersion of ZnO NPs highlights the effectiveness of the proposed methodology for the in-situ synthesis and immobilization of ZnO NPs on the PES HF membrane surface.

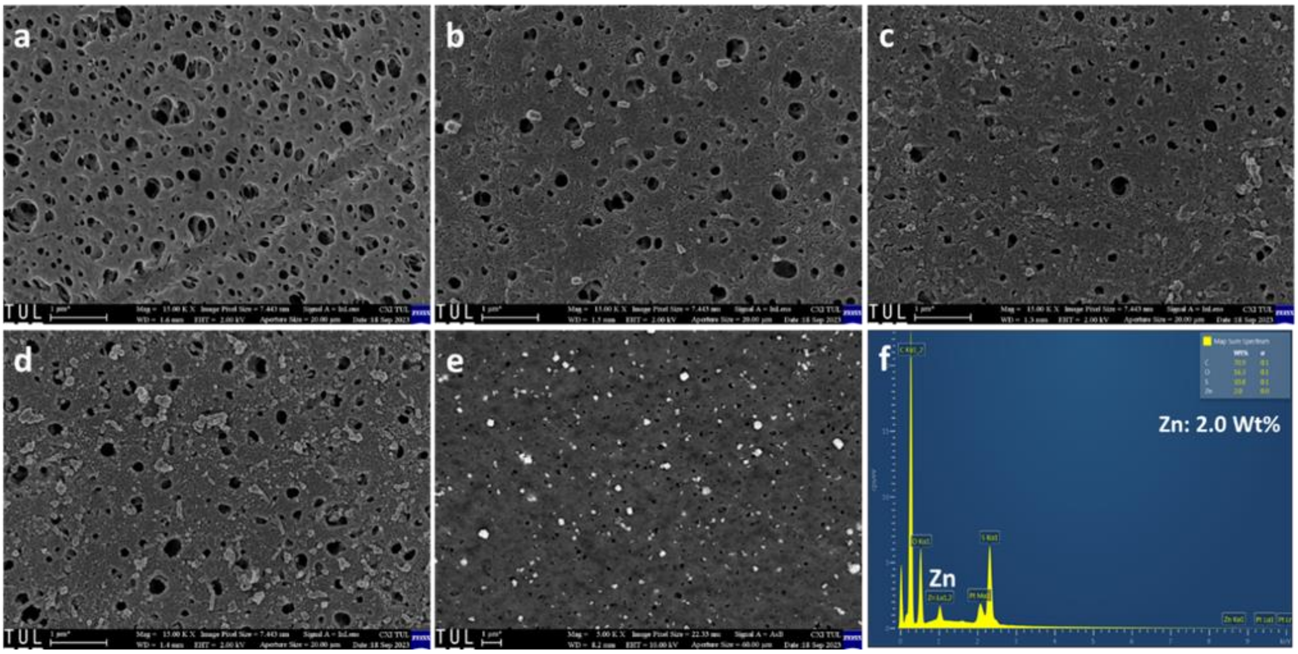

Fig. 18. SEM analysis of: a) pristine PES, b) PDA {1.0 h}, c) PDA {2.5 h}, d) PDA {4.0 h} incorporated ZnO NPs modified PES HF membrane, and EDX-coupled e) high contrast image and f) elemental analysis of PDA (1.0 h) incorporated ZnO NPs modified PES HF membrane.

4.3.2.2. Permeability, and critical flux evaluation

The permeability of pristine and surface-modified PES HF membranes with DI water was assessed prior to the filtration of activated sludge (AS) by analyzing flux versus TMP curves, which demonstrated a high degree of accuracy with R^2 values up to 0.99. The time-dependent growth of the PDA layer on the PES HF membrane resulted in reduced pore sizes as polymerization time increased, consequently lowering the permeability of the modified membranes. Specifically, permeability decreased from 394 ($L \cdot m^{-2} \cdot h^{-1} \cdot bar^{-1}$) for the pristine PES membrane to 342, 284, and 272 ($L \cdot m^{-2} \cdot h^{-1} \cdot bar^{-1}$) after PDA treatments of 1.0, 2.5, and 4.0 hours, respectively, while maintaining a consistent amount of ZnO NPs. Despite these reductions, the modified membranes still exhibited sufficient permeability for wastewater treatment applications and demonstrated potential for use as submerged membrane modules in MBRs.

Critical fluxes of both pristine and surface-modified PES HF membranes were further evaluated using the flux step test. Municipal activated sludge (AS) was sourced from the central WWTP in Liberec, Czechia, and used for the determination of the fouling rate and, consequently, critical flux in a lab-scale membrane bioreactor (MBR). Fig. 19a shows the changes in TMP as the flux was progressively increased during 10-minute filtration cycles, with each cycle consisting of 9 minutes of filtration and 1 minute of relaxation. Previous research highlighted the time-dependent nature of PDA polymerization on the membrane surface, resulting in a decrease in porosity [32]. Consistent with this, the current results reveal that extending the PDA polymerization time led to an increase in TMP, attributed to the reduction in pore size and porosity of the membranes. Fig. 19b and Fig. 19c illustrate the changes in flux and permeability over time. Membrane fluxes steadily rose until reaching approximately 30 ($L\cdot m^{-2}\cdot h^{-1}\cdot bar^{-1}$) after 1 hour of filtration, at which point the primary differences among membranes became apparent. Flux continued to increase, reaching up to 40.0 ($L\cdot m^{-2}\cdot h^{-1}\cdot bar^{-1}$) for the pristine PES HF membrane which showed the highest flux at around 42.5 ($L\cdot m^{-2}\cdot h^{-1}\cdot bar^{-1}$), and the PES membrane modified with 4.0-hour PDA polymerization and incorporated ZnO NPs exhibited the lowest flux at about 36.7 ($L\cdot m^{-2}\cdot h^{-1}\cdot bar^{-1}$). Analysis of the fouling rate (FR) indicated that both the pristine PES and the PDA (1.0 h) + ZnO NPs modified membranes surpassed the threshold of 0.5 $mbar\cdot min^{-1}$ at higher fluxes, around 22 ($L\cdot m^{-2}\cdot h^{-1}\cdot bar^{-1}$), whereas the PDA (2.5 h) and PDA (4.0 h) + ZnO NPs modified membranes reached this threshold at lower fluxes, approximately 19 ($L\cdot m^{-2}\cdot h^{-1}\cdot bar^{-1}$) and 16 ($L\cdot m^{-2}\cdot h^{-1}\cdot bar^{-1}$), respectively. This suggests that the PES HF membrane modified with 1-hour PDA polymerization and incorporated ZnO NPs exhibited the least fouling tendency during MBR operation.

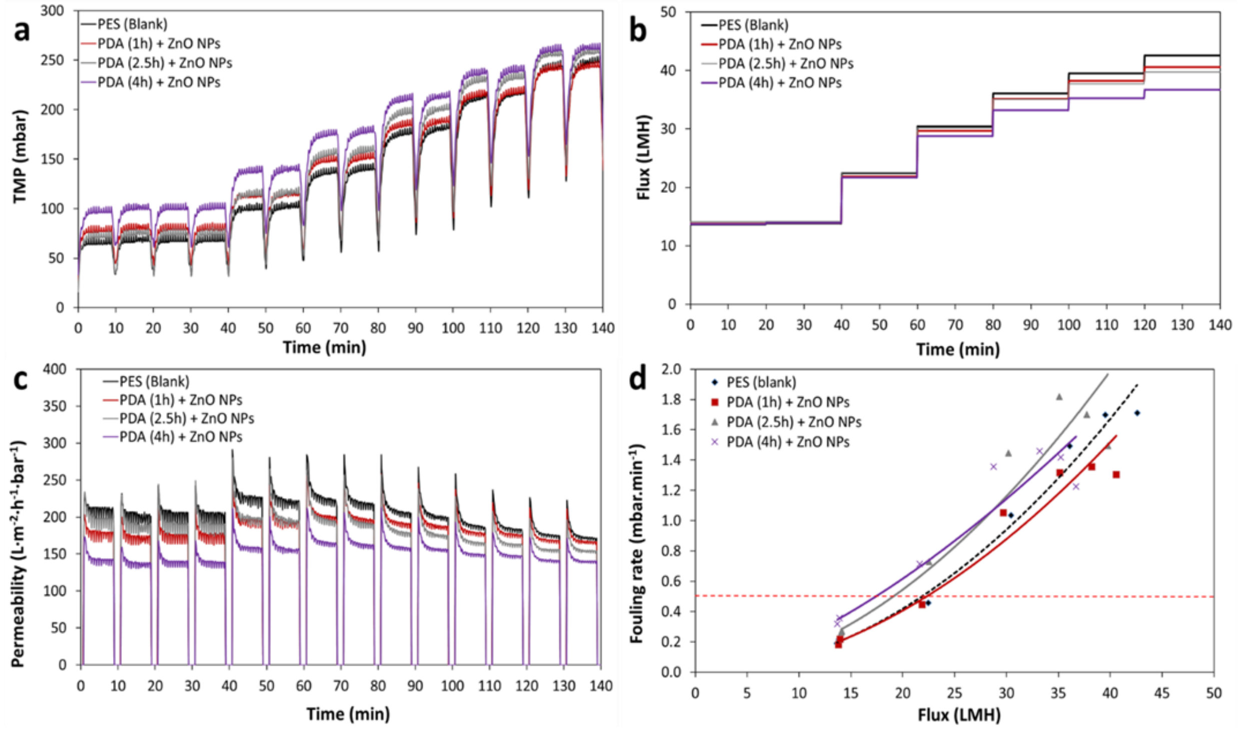

Fig. 19. Results of the flux step measurement using pristine and surface-modified PES HF membranes.

4.3.2.3. Antimicrobial properties

A quantitative analysis of PES HF membranes, conducted at various time intervals following microbial assessment through dynamic contact procedures and subsequent 48-hour incubation at

37 °C, revealed enhanced antimicrobial properties in surface-modified PES HF membranes incorporating ZnO NPs compared to the pristine membrane, for both tested bacteria: *E. coli* and *Staphylococcus sp.* (Fig. 20). While PDA surface modification reduced CFU relative to the pristine membrane, indicating diminished bacterial adhesion, the PDA-modified membranes exhibited only slightly antimicrobial activity, with reductions of 1.49% and 4.59% against *E. coli* after 2 and 5 hours, respectively. A similar trend was observed against *Staphylococcus sp.*, with no significant antimicrobial effect relative to the pristine membrane. Notable reductions were only achieved after 24 hours, reaching 58.54% for *E. coli* and 75% for *Staphylococcus sp.*. In contrast, the incorporation of ZnO NPs significantly enhanced the antimicrobial performance, achieving a 100% reduction in bacterial presence within 5 hours for *E. coli* and 24 hours for *Staphylococcus sp.* This highlights the significant contribution of ZnO NPs to the membranes' antibacterial efficacy.

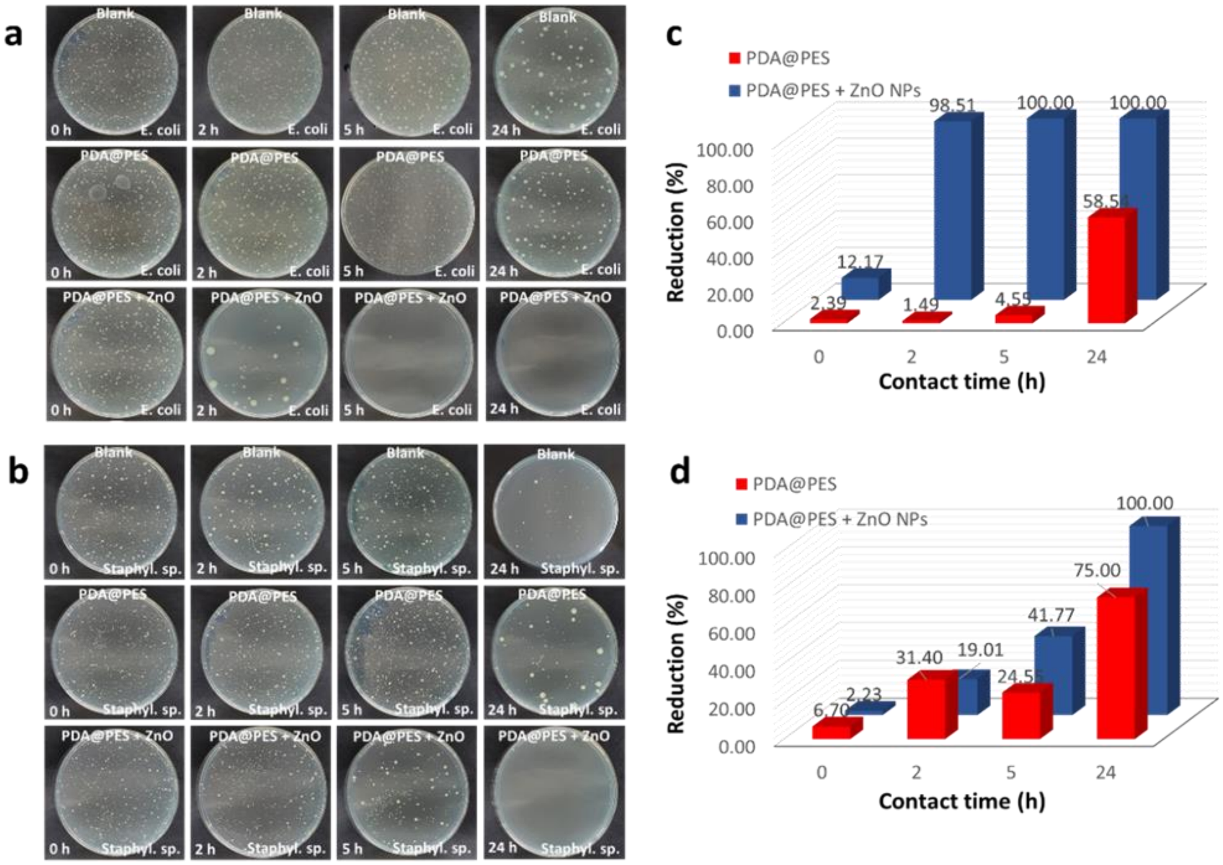

Fig. 20. Antibacterial evaluation: (a) CFU assay images and (c) reduction diagrams of *E. coli*, along with (b) CFU assay images and (d) reduction diagrams of *Staphylococcus sp.* cultured in contact with pristine and surface-modified PES membranes at contact times of 0.0, 2.0, 5.0, and 24.0 hours.

4.3.3. Summary

The study successfully demonstrated the uniform coverage of PDA nanospheres and the in-situ synthesis and immobilization of ZnO NPs on the surface of PES HF membranes, as confirmed by surface morphology and elemental analysis. The PDA-modified PES membranes incorporating ZnO NPs exhibited anti-biofouling properties, achieving a 100% reduction in bacterial cells within just 5 hours for *E. coli* and 24 hours for *Staphylococcus sp*. A strong correlation was established between the membranes' surface characteristics and their performance in MBR applications. Permeability tests with DI water and flux step analyses revealed that increased PDA polymerization time led to reduced pore size, as observed via SEM imaging, and a corresponding decrease in DI water permeability. Specifically, while the pristine PES HF membrane exhibited a permeability of 394 ($L \cdot m^{-2} \cdot h^{-1} \cdot bar^{-1}$), the PDA-treated membranes (1.0 h, 2.5 h, and 4.0 h) showed progressively lower permeabilities of 342, 284, and 272 ($L \cdot m^{-2} \cdot h^{-1} \cdot bar^{-1}$), respectively. Among the modified membranes, the PDA (1.0 h) + ZnO NPs membrane showed optimal performance, maintaining a critical flux comparable to the pristine PES HF membrane (approximately 22 ($L \cdot m^{-2} \cdot h^{-1}$)) while demonstrating superior antibacterial activity. This highlights the potential of PDA-modified PES membranes with ZnO NPs as a promising solution for enhanced anti-biofouling performance in wastewater treatment applications.

5. Conclusions

This research aimed to enhance membrane performance for advanced wastewater treatment by modifying membrane surfaces to repel or reduce interactions with microorganisms, dissolved organic matter, proteins, and suspended solids. The study explored three primary methodologies, highlighting their distinct advantages and limitations, while also addressing the need for continuous improvement. The first chapter focused on superhydrophobic surface coating, which involved the application of a biomimetic coating on PET fabric surfaces. This modification employed a hierarchical composition of PDA, in-situ synthesized ZnO NPs, and a non-fluorinated silane layer, achieving remarkable surface hydrophobicity. With a WCA of 150°-160° and a roll-off angle of 2°-6°, the superhydrophobic membranes demonstrated high organic solvent-water separation efficiency (≥90%), significant bacterial repulsion, and robust stability under mechanical and chemical stresses. However, their limited permeability and reduced performance in aqueous environments, particularly in MBR applications, underscored the need for alternative strategies that combine anti-biofouling properties with enhanced hydrophilicity.

The second chapter introduced superhydrophilic surface modification of HF membranes through air-stimulated PDA polymerization and ZnO NP incorporation. This method transformed PTFE membranes into highly hydrophilic surfaces, improving fouling resistance, and bacterial reduction capabilities. FRR increased to 76% after PDA coating and 68% after ZnO NP immobilization, while fouling tendencies decreased significantly. Moreover, the modified membranes achieved 100% bacterial reduction against *E. coli* and *Staphylococcus sp.* within short inoculation times. Despite these benefits, long-term performance under higher flux than the critical flux conditions remained a challenge, highlighting the importance of optimizing operational parameters to prevent fouling.

In the third chapter, critical flux evaluation was conducted to optimize membrane performance, focusing on the fouling behavior of PDA-modified PES HF membranes incorporating ZnO NPs. These modifications achieved 100% bacterial reduction within 5 hours for *E. coli* and 24 hours for *Staphylococcus sp.*, while retaining a critical flux comparable to pristine membranes (~22 $L \cdot m^{-2} \cdot h^{-1}$). However, balancing optimal permeability and biofouling resistance remains a challenge, necessitating further optimization of all modification parameters to enhance anti-biofouling efficacy and maximize permeability.

Comparative analysis of these methodologies highlights their complementary roles in wastewater treatment applications. Superhydrophobic coatings are highly effective for separating organic solvents and oily wastewater but exhibit lower permeability, limiting their suitability for MBR systems. In contrast, superhydrophilic modifications enhance permeability and anti-biofouling properties, making them better suited for MBR applications. In addition, maintaining flux below the critical threshold remains essential to mitigate fouling and ensure long-term operational stability. Future research should aim to integrate the advantages of superhydrophilic properties with the evaluation and optimization of modification parameters to improve membrane performance. Furthermore, optimizing operational parameters, particularly critical flux management, will be vital to maximizing efficiency and extending membrane longevity in advanced wastewater treatment systems.

6. Outline of the future experiments

The necessity of surface modification for submerged membranes in bioreactors, along with its influence on properties like critical flux, highlights the importance of optimizing modification parameters. Accordingly, the future plan is focused on optimizing these parameters to develop modified membranes with improved performance and reduced fouling tendencies.

Another plan is to conduct long-term testing of the modified membranes to evaluate their performance within the MBR and to characterize the quality of the treated effluent.

7. Publications

- ✓ Highly Stable, Flexible, Anticorrosive Coating of Metalized Nonwoven Textiles for Durable EMI Shielding and Thermal Properties
  MZ Khan, **H Taghavian**, X Zhang, J Militky, A Ali, J Wiener, V Tunáková, ...
  ACS Omega 2025 10 (8), 8127-8139 (2025).

- ✓ UV-Activated TiO_2-Coated Carbon Felt for Photocatalytic Dye Degradation and Antibacterial Applications
  Y Wang, J Omsinsombon, N Prateepmaneerak, S Li, G Zhu, MZ Khan, **H Taghavian**, M Venkataraman, J Militký, A Chaiyasat.
  Surfaces and Interfaces, 106018 (2025).

- ✓ Green superhydrophobic surface engineering of PET fabric for advanced water-solvent separation
  H Taghavian, MZ Khan, J Wiener, J Militky, B Tomkova, M Venkataraman, ...
  Progress in Organic Coatings 197, 108842 (2024).

- ✓ Green in-situ immobilization of ZnO nanoparticles for functionalization of polyester fabrics
  MZ Khan, **H Taghavian**, J Wiener, J Militky, Y Wang, B Tomkova, M Cernik, ...
  Surfaces and Interfaces 55, 105336 (2024).

- ✓ A Novel Organic–Inorganic-Nanocomposite-Based Reduced Graphene Oxide as an Efficient Nanosensor for NO_2 Detection
  M Khaleghiabbasabadi, **H Taghavian**, P Gholami, S Khodabakhshi, ...
  Nanomaterials 14 (24), 1983 (2024).

- ✓ "A risk-based soft sensor for failure rate monitoring in water distribution network via adaptive neuro-fuzzy interference systems"
  Mohammad Gheibi, Reza Moezzi, **Hadi Taghavian**, Stanisław Wacławek, Nima Emrani, Mohsen Mohtasham, Masoud Khaleghiabbasabadi, Jan Koci, Cheryl S. Y. Yeap & Jindrich Cyrus
  Scientific Reports 13, 12200 (2023).

- ✓ "Advanced (bio) fouling resistant surface modification of PTFE hollow-fiber membranes for water treatment"
  H Taghavian, M ČERNÍK, L DVOŘÁK
  Scientific Reports 13, 11871 (2023).

- ✓ "Effect of microwave power on bactericidal and UV protection properties of the ZnO nanorods grown cotton fabrics"
  MZ Khan, **H Taghavian**, M Fijalkowski, J Militky, B Tomkova, ...
  Colloids and Surfaces A: Physicochemical and Engineering Aspects 664, 131135 (2023).

- ✓ "Exterior surface characterization of the novel surface modified PES HF membrane applicable in bioreactor"
  H Taghavian, M ČERNÍK, L DVOŘÁK
  Proceedings 15th International Conference on Nanomaterials - Research & Application, (2023).

- ✓ "A Smart Bioreactor-based Production and Distribution System for Spirulina Algae in Developed Countries"
  M Gheibi, R Moezzi, M Khaleghiabbasabadi, **H Taghavian**, TM Vu
  International Journal of Innovative Technology and Interdisciplinary Sciences (2023).

- ✓ “Intelligent Estimation of Total Suspended Solids (TSS) in Wastewater Treatment Plants Utilizing Non-Liner Regression Analysis”
  M Gheibi, R Moezzi, M Khaleghiabbasabadi, **H Taghavian**, K Dhoska
  Journal of Transactions in Systems Engineering 1 (1), 50-55 (2023).

- ✓ “The operation of urban water treatment plants: a review of smart dashboard frameworks”
  A Kiyan, M Gheibi, M Akrami, R Moezzi, K Behzadian, **H Taghavian**
  Environmental Industry Letters 1 (1), (2023).

- ✓ “Design of a Decision Support System to Operate a NO_2 Gas Sensor Using Machine Learning, Sensitive Analysis and Conceptual Control Process Modelling”
  M Gheibi, **H Taghavian**, R Moezzi, S Waclawek, J Cyrus, ...
  Chemosensors 11 (2), 126 (2023).

- ✓ “Superhydrophilic surface modification of PTFE hollow-fiber membrane with advanced biofouling properties for water purification”
  H Taghavian, M ČERNÍK, L DVOŘÁK
  Proceedings 14th International Conference on Nanomaterials - Research & Application, 91-96 (2022).

8. References

[1] S. Kim *et al.*, ‘Review of adsorption–membrane hybrid systems for water and wastewater treatment’, *Chemosphere*, vol. 286, p. 131916, Jan. 2022, doi: 10.1016/j.chemosphere.2021.131916.

[2] R. Sengur-Tasdemir, G. M. Urper-Bayram, T. Turken, E. Ates-Genceli, V. V. Tarabara, and I. Koyuncu, ‘HF nanofiltration membranes for surface water treatment: Performance evaluation at the pilot scale’, *Journal of Water Process Engineering*, vol. 42, p. 102100, Aug. 2021, doi: 10.1016/j.jwpe.2021.102100.

[3] H. S. Zakria *et al.*, ‘Removal of bisphenol A from synthetic and treated sewage wastewater using magnetron sputtered CuxO/PVDF thin film photocatalytic HF membrane’, *Journal of Water Process Engineering*, vol. 51, p. 103425, Feb. 2023, doi: 10.1016/j.jwpe.2022.103425.

[4] L. Zhang *et al.*, ‘The performance of electrode ultrafiltration membrane bioreactor in treating cosmetics wastewater and its anti-fouling properties’, *Environmental Research*, vol. 206, p. 112629, Apr. 2022, doi: 10.1016/j.envres.2021.112629.

[5] I. Kim *et al.*, ‘An efficient continuous quorum quenching feed to mitigate membrane biofouling in membrane bioreactors: Strain 1A1 (extracellular) versus strain BH4 (intracellular)’, *Journal of Water Process Engineering*, vol. 52, p. 103594, Apr. 2023, doi: 10.1016/j.jwpe.2023.103594.

[6] F. Dolatkhah, T. Mohammadi, and M. A. Tofighy, ‘Polysulfone HF membrane containing charcoal-carbon nanomaterial for wastewater treatment in membrane bioreactor’, *Journal of Water Process Engineering*, vol. 50, p. 103222, Dec. 2022, doi: 10.1016/j.jwpe.2022.103222.

[7] Z. Yang, Q. N. Tran, and X. Jin, ‘Ultrafiltration of aerobic granular sludge bioreactor effluent: Fouling potentials and properties’, *Journal of Water Process Engineering*, vol. 47, p. 102805, Jun. 2022, doi: 10.1016/j.jwpe.2022.102805.

[8] A. K. Wardani, D. Ariono, Subagjo, and I. G. Wenten, ‘Hydrophilic modification of polypropylene ultrafiltration membrane by air-assisted polydopamine coating’, *Polymers for Advanced Techs*, vol. 30, no. 4, pp. 1148–1155, Apr. 2019, doi: 10.1002/pat.4549.

[9] L. Shao, Z. X. Wang, Y. L. Zhang, Z. X. Jiang, and Y. Y. Liu, ‘A facile strategy to enhance PVDF

ultrafiltration membrane performance via self-polymerized polydopamine followed by hydrolysis of ammonium fluotitanate', *Journal of Membrane Science*, vol. 461, pp. 10–21, Jul. 2014, doi: 10.1016/j.memsci.2014.03.006.

[10] H. Song, H. Yu, L. Zhu, L. Xue, D. Wu, and H. Chen, 'Durable hydrophilic surface modification for PTFE HF membranes', *Reactive and Functional Polymers*, vol. 114, pp. 110–117, May 2017, doi: 10.1016/j.reactfunctpolym.2017.03.010.

[11] Z. An, F. Dai, C. Wei, Y. Zhao, and L. Chen, 'Polydopamine/cysteine surface modified hemocompatible poly(vinylidene fluoride) HF membranes for hemodialysis', *J Biomed Mater Res*, vol. 106, no. 8, pp. 2869–2877, Nov. 2018, doi: 10.1002/jbm.b.34106.

[12] F. Galiano *et al.*, 'Novel low-fouling membranes from lab to pilot application in textile wastewater treatment', *Journal of Colloid and Interface Science*, vol. 515, pp. 208–220, Apr. 2018, doi: 10.1016/j.jcis.2018.01.009.

[13] Q. Zhou, S. Liu, J. She, X. Wang, X. Lu, and C. Wu, 'In-situ aeration-assisted polydopamine/polyethyleneimine copolymerization and deposition for rapid and uniform membrane modification', *Journal of Membrane Science*, vol. 657, p. 120662, Sep. 2022, doi: 10.1016/j.memsci.2022.120662.

[14] J. H. Kim, M. K. Joshi, J. Lee, C. H. Park, and C. S. Kim, 'Polydopamine-assisted immobilization of hierarchical zinc oxide nanostructures on electrospun nanofibrous membrane for photocatalysis and antimicrobial activity', *Journal of Colloid and Interface Science*, vol. 513, pp. 566–574, Mar. 2018, doi: 10.1016/j.jcis.2017.11.061.

[15] H. Monclus, S. Zacharias, A. Santos, M. Pidou, and S. Judd, 'Criticality of Flux and Aeration for a HF Membrane Bioreactor', *Separation Science and Technology*, vol. 45, no. 7, pp. 956–961, Apr. 2010, doi: 10.1080/01496391003666197.

[16] H. Monclús, G. Ferrero, G. Buttiglieri, J. Comas, and I. Rodriguez-Roda, 'Online monitoring of membrane fouling in submerged MBRs', *Desalination*, vol. 277, no. 1–3, pp. 414–419, Aug. 2011, doi: 10.1016/j.desal.2011.04.055.

[17] D. Jenkins, J. Wanner, and International Water Association, Eds., *Activated sludge - 100 years and counting: papers delivered at the Conference 'Activated Sludge ... 100 Years and Counting!' held in Essen, Germany, June 12th to 14th, 2014*, 1. publ. London: IWA Publishing, 2014.

[18] D. Singh *et al.*, 'Biofouling in Membrane Bioreactors: Mechanism, Interactions and Possible Mitigation Using Biosurfactants', *Appl Biochem Biotechnol*, vol. 195, no. 3, pp. 2114–2133, Mar. 2023, doi: 10.1007/s12010-022-04261-4.

[19] A. Raszka, M. Chorvatova, and J. Wanner, 'The role and significance of extracellular polymers in activated sludge. Part I: Literature review', *Acta hydrochim. hydrobiol.*, vol. 34, no. 5, pp. 411–424, Oct. 2006, doi: 10.1002/aheh.200500640.

[20] E. Zolghadr *et al.*, 'An ultrasonic-assisted rapid approach for sustainable fabrication of antibacterial and anti-biofouling membranes via metal-organic frameworks', *Materials Today Chemistry*, vol. 26, p. 101044, Dec. 2022, doi: 10.1016/j.mtchem.2022.101044.

[21] M. Pakizeh, F. Azinfar, M. Safarnia, and F. Raji, 'The effects of TiO_2 nanoparticles and polydopamine on the structure, separation, and antifouling properties of PPSU membrane', *Separation Science and Technology*, vol. 57, no. 11, pp. 1788–1799, Jul. 2022, doi: 10.1080/01496395.2021.2006230.

[22] S. Jahankhah, M. M. Sabzehmeidani, M. Ghaedi, K. Dashtian, and H. Abbasi-Asl, 'Fabrication polyvinyl chloride mixed matrix membrane via embedding Fe3O4/ polydopamine /Ag nanocomposite for water treatment', *Materials Science and Engineering: B*, vol. 285, p. 115935, Nov. 2022, doi:

10.1016/j.mseb.2022.115935.

[23] S. Yang *et al.*, ‘Graphene oxide and reduced graphene oxide coated cotton fabrics with opposite wettability for continuous oil/water separation’, *Separation and Purification Technology*, vol. 259, p. 118095, Mar. 2021, doi: 10.1016/j.seppur.2020.118095.

[24] W. Ma *et al.*, ‘Dual pH- and ammonia-vapor-responsive electrospun nanofibrous membranes for oil-water separations’, *Journal of Membrane Science*, vol. 537, pp. 128–139, Sep. 2017, doi: 10.1016/j.memsci.2017.04.063.

[25] N. Y. Abu-Thabit *et al.*, ‘Rapid, Sustainable, and Versatile Strategy Towards Fabricating Superhydrophobic Cotton Textile Membranes for Separation of Emulsified and Stratified Oil/Water Mixtures’, *Separation and Purification Technology*, vol. 330, p. 125352, Feb. 2024, doi: 10.1016/j.seppur.2023.125352.

[26] D. Johnson, F. Galiano, S. A. Deowan, J. Hoinkis, A. Figoli, and N. Hilal, ‘Adhesion forces between humic acid functionalized colloidal probes and polymer membranes to assess fouling potential’, *Journal of Membrane Science*, vol. 484, pp. 35–46, Jun. 2015, doi: 10.1016/j.memsci.2015.03.018.

[27] X. Li, H. Shan, M. Cao, and B. Li, ‘Mussel-inspired modification of PTFE membranes in a miscible THF-Tris buffer mixture for oil-in-water emulsions separation’, *Journal of Membrane Science*, vol. 555, pp. 237–249, Jun. 2018, doi: 10.1016/j.memsci.2018.03.010.

[28] Y. Zhang, F. Shen, W. Cao, and Y. Wan, ‘Hydrophilic/hydrophobic Janus membranes with a dual-function surface coating for rapid and robust membrane distillation desalination’, *Desalination*, vol. 491, p. 114561, Oct. 2020, doi: 10.1016/j.desal.2020.114561.

[29] H.-Y. Fu, P.-C. Xu, G.-H. Huang, T. Chai, M. Hou, and P.-F. Gao, ‘Effects of aeration parameters on effluent quality and membrane fouling in a submerged membrane bioreactor using Box–Behnken response surface methodology’, *Desalination*, vol. 302, pp. 33–42, Sep. 2012, doi: 10.1016/j.desal.2012.06.018.

[30] M. B. Asif, R. Habib, S. Iftekhar, Z. Khan, and N. Majeed, ‘Optimization of the operational parameters in a submerged membrane bioreactor using Box Behnken response surface methodology: membrane fouling control and effluent quality’, *Desalination and Water Treatment*, vol. 82, pp. 26–38, Jul. 2017, doi: 10.5004/dwt.2017.20998.

[31] H. Taghavian *et al.*, ‘Green superhydrophobic surface engineering of PET fabric for advanced water-solvent separation’, *Progress in Organic Coatings*, vol. 197, p. 108842, Dec. 2024, doi: 10.1016/j.porgcoat.2024.108842.

[32] H. Taghavian, M. Černík, and L. Dvořák, ‘Advanced (bio)fouling resistant surface modification of PTFE hollow-fiber membranes for water treatment’, *Sci Rep*, vol. 13, no. 1, p. 11871, Jul. 2023, doi: 10.1038/s41598-023-38764-9.

[33] S. Sadeghi, M. Montazer, and F. Dadashian, ‘Insights into the hexamine-assisted ZnO based-MOFs formation on PET fabric for improved self-cleaning, flame retardant, and hydrophilic properties’, *Progress in Organic Coatings*, vol. 192, p. 108458, Jul. 2024, doi: 10.1016/j.porgcoat.2024.108458.

[34] B. Nozari, M. Montazer, and M. Mahmoudi Rad, ‘Stable ZnO/SiO2 nano coating on polyester for anti-bacterial, self-cleaning and flame retardant applications’, *Materials Chemistry and Physics*, vol. 267, p. 124674, Jul. 2021, doi: 10.1016/j.matchemphys.2021.124674.

[35] U. Daood, C. Yiu, M. F. Burrow, L.-N. Niu, and F. R. Tay, ‘Effect of a novel quaternary ammonium silane on dentin protease activities’, *Journal of Dentistry*, vol. 58, pp. 19–27, Mar. 2017, doi: 10.1016/j.jdent.2017.01.001.

[36] P. Yang, M. Chin, and C. Lee, ‘Interaction of Hyaluronic Acid (HA) with Organosilicon (Si-QAC)

Modified Magnetite for HA Recovery', *Separation Science and Technology*, vol. 42, no. 8, pp. 1747–1760, Jun. 2007, doi: 10.1080/01496390701242160.

[37] D. Cheng *et al.*, 'Hydrothermal growing of cluster-like ZnO nanoparticles without crystal seeding on PET films via dopamine anchor', *Applied Surface Science*, vol. 467–468, pp. 534–542, Feb. 2019, doi: 10.1016/j.apsusc.2018.10.177.

[38] V. R. Shinde *et al.*, 'Growth of Shape- and Size-Selective Zinc Oxide Nanorods by a Microwave-Assisted Chemical Bath Deposition Method: Effect on Photocatalysis Properties', *Chemistry A European J*, vol. 16, no. 34, pp. 10569–10575, Sep. 2010, doi: 10.1002/chem.200903370.

[39] K. Edalati, A. Shakiba, J. Vahdati-Khaki, and S. M. Zebarjad, 'Low-temperature hydrothermal synthesis of ZnO nanorods: Effects of zinc salt concentration, various solvents and alkaline mineralizers', *Materials Research Bulletin*, vol. 74, pp. 374–379, Feb. 2016, doi: 10.1016/j.materresbull.2015.11.001.

[40] H. Zhang, D. Yang, X. Ma, N. Du, J. Wu, and D. Que, 'Straight and Thin ZnO Nanorods: Hectogram-Scale Synthesis at Low Temperature and Cathodoluminescence', *J. Phys. Chem. B*, vol. 110, no. 2, pp. 827–830, Jan. 2006, doi: 10.1021/jp055351k.

[41] M. Mecozzi and L. Nisini, 'The differentiation of biodegradable and non-biodegradable polyethylene terephthalate (PET) samples by FTIR spectroscopy: A potential support for the structural differentiation of PET in environmental analysis', *Infrared Physics & Technology*, vol. 101, pp. 119–126, Sep. 2019, doi: 10.1016/j.infrared.2019.06.008.

[42] A. Thakur, S. Ranote, D. Kumar, K. K. Bhardwaj, R. Gupta, and G. S. Chauhan, 'Synthesis of a PEGylated Dopamine Ester with Enhanced Antibacterial and Antifungal Activity', *ACS Omega*, vol. 3, no. 7, pp. 7925–7933, Jul. 2018, doi: 10.1021/acsomega.8b01099.

[43] Vikas, V. Lahariya, and R. K. Tamrakar, 'Structural, optical and thermoluminescence study of annealed zinc aluminate spinel nanophosphor', *J Mater Sci: Mater Electron*, vol. 34, no. 31, p. 2117, Nov. 2023, doi: 10.1007/s10854-023-11519-y.

[44] University of Ljubljana, Faculty of Natural Sciences and Engineering, Department of Textiles, Graphic Arts and Design, Snežniška 5, 1000 Ljubljana, Slovenia *et al.*, 'Application of Stimuli Responsive Microgel for Creation of Smart Cotton Fabric with Antibacterial Properties', *TEK*, vol. 59, no. 2, pp. 142–148, May 2016, doi: 10.14502/Tekstilec2016.59.142-148.

[45] E. S. Ates and H. E. Unalan, 'Zinc oxide nanowire enhanced multifunctional coatings for cotton fabrics', *Thin Solid Films*, vol. 520, no. 14, pp. 4658–4661, May 2012, doi: 10.1016/j.tsf.2011.10.073.

[46] X. Dong *et al.*, 'A self-roughened and biodegradable superhydrophobic coating with UV shielding, solar-induced self-healing and versatile oil–water separation ability', *J. Mater. Chem. A*, vol. 7, no. 5, pp. 2122–2128, 2019, doi: 10.1039/C8TA10869B.

[47] X. Luo, Y. Weng, S. Wang, J. Du, H. Wang, and C. Xu, 'Superhydrophobic and oleophobic textiles with hierarchical micro-nano structure constructed by sol–gel method', *J Sol-Gel Sci Technol*, vol. 89, no. 3, pp. 820–829, Mar. 2019, doi: 10.1007/s10971-019-04927-2.

[48] E. Pakdel, J. Wang, S. Kashi, L. Sun, and X. Wang, 'Advances in photocatalytic self-cleaning, superhydrophobic and electromagnetic interference shielding textile treatments', *Advances in Colloid and Interface Science*, vol. 277, p. 102116, Mar. 2020, doi: 10.1016/j.cis.2020.102116.

[49] M. Beitollahpoor, M. Farzam, and N. S. Pesika, 'Friction force-based measurements for simultaneous determination of the wetting properties and stability of superhydrophobic surfaces', *Journal of Colloid and Interface Science*, vol. 648, pp. 161–168, Oct. 2023, doi: 10.1016/j.jcis.2023.05.161.

[50] M. Zaman Khan *et al.*, 'Recent advances in superhydrophobic surfaces for practical applications: A

review’, *European Polymer Journal*, vol. 178, p. 111481, Sep. 2022, doi: 10.1016/j.eurpolymj.2022.111481.

[51] D. Hill, H. Attia, A. R. Barron, and S. Alexander, ‘Size and morphology dependent surface wetting based on hydrocarbon functionalized nanoparticles’, *Journal of Colloid and Interface Science*, vol. 543, pp. 328–334, May 2019, doi: 10.1016/j.jcis.2019.02.058.

[52] S. Parvate, P. Dixit, and S. Chattopadhyay, ‘Superhydrophobic Surfaces: Insights from Theory and Experiment’, *J. Phys. Chem. B*, vol. 124, no. 8, pp. 1323–1360, Feb. 2020, doi: 10.1021/acs.jpcb.9b08567.

[53] J.-W. Song, M.-C. Ma, and L.-W. Fan, ‘Understanding the Temperature Dependence of Contact Angles of Water on a Smooth Hydrophobic Surface under Pressurized Conditions: An Experimental Study’, *Langmuir*, vol. 36, no. 32, pp. 9586–9595, Aug. 2020, doi: 10.1021/acs.langmuir.0c01671.

[54] B. Wang *et al.*, ‘Preparation of superhydrophobic nylon-56/cotton-interwoven fabric with dopamine-assisted use of thiol–ene click chemistry’, *RSC Adv.*, vol. 11, no. 18, pp. 10699–10709, 2021, doi: 10.1039/D1RA00410G.

[55] M. Z. Khan, V. Baheti, J. Militky, J. Wiener, and A. Ali, ‘Self-cleaning properties of polyester fabrics coated with flower-like TiO_2 particles and trimethoxy (octadecyl)silane’, *Journal of Industrial Textiles*, vol. 50, no. 4, pp. 543–565, Oct. 2020, doi: 10.1177/1528083719836938.

[56] D. Ashok *et al.*, ‘Superhydrophobic Surfaces to Combat Bacterial Surface Colonization’, *Adv Materials Inter*, vol. 10, no. 24, p. 2300324, Aug. 2023, doi: 10.1002/admi.202300324.

[57] J. Wang, F. Han, and S. Zhang, ‘Durably superhydrophobic textile based on fly ash coating for oil/water separation and selective oil removal from water’, *Separation and Purification Technology*, vol. 164, pp. 138–145, May 2016, doi: 10.1016/j.seppur.2016.03.038.

[58] F. Sun, J. Lu, Y. Wang, J. Xiong, C. Gao, and J. Xu, ‘Reductant-assisted polydopamine-modified membranes for efficient water purification’, *Front. Chem. Sci. Eng.*, vol. 15, no. 1, pp. 109–117, Feb. 2021, doi: 10.1007/s11705-020-1987-9.

[59] M. Sianipar, S. H. Kim, C. Min, L. D. Tijing, and H. K. Shon, ‘Potential and performance of a polydopamine-coated multiwalled carbon nanotube/polysulfone nanocomposite membrane for ultrafiltration application’, *Journal of Industrial and Engineering Chemistry*, vol. 34, pp. 364–373, Feb. 2016, doi: 10.1016/j.jiec.2015.11.025.

[60] Y. Bi, B. Han, S. Zimmerman, F. Perreault, S. Sinha, and P. Westerhoff, ‘Four release tests exhibit variable silver stability from nanoparticle-modified reverse osmosis membranes’, *Water Research*, vol. 143, pp. 77–86, Oct. 2018, doi: 10.1016/j.watres.2018.06.036.

[61] S. Liu, F. Fang, J. Wu, and K. Zhang, ‘The anti-biofouling properties of thin-film composite nanofiltration membranes grafted with biogenic silver nanoparticles’, *Desalination*, vol. 375, pp. 121–128, Nov. 2015, doi: 10.1016/j.desal.2015.08.007.

[62] M. Sri Abirami Saraswathi, R. Kausalya, N. J. Kaleekkal, D. Rana, and A. Nagendran, ‘BSA and humic acid separation from aqueous stream using polydopamine coated PVDF ultrafiltration membranes’, *Journal of Environmental Chemical Engineering*, vol. 5, no. 3, pp. 2937–2943, Jun. 2017, doi: 10.1016/j.jece.2017.05.051.

[63] P. Zhang *et al.*, ‘Modification of PVDF HF membrane by co-deposition of PDA/MPC-co-AEMA for membrane distillation application with anti-fouling and anti-scaling properties’, *Journal of Membrane Science*, vol. 636, p. 119596, Oct. 2021, doi: 10.1016/j.memsci.2021.119596.

[64] Y. Chen, K.-J. Lu, C. Z. Liang, and T.-S. Chung, ‘Mechanically strong Janus tri-bore HF membranes with asymmetric pores for anti-wetting and anti-fouling membrane distillation’, *Chemical Engineering Journal*,

vol. 429, p. 132455, Feb. 2022, doi: 10.1016/j.cej.2021.132455.

[65] M. Sun, Y. Su, C. Mu, and Z. Jiang, ‘Improved Antifouling Property of PES Ultrafiltration Membranes Using Additive of Silica−PVP Nanocomposite’, *Ind. Eng. Chem. Res.*, vol. 49, no. 2, pp. 790–796, Jan. 2010, doi: 10.1021/ie900560e.

[66] A. M. Zhukov, V. I. Solodilov, I. V. Tretyakov, E. A. Burakova, and G. Yu. Yurkov, ‘The Effect of the Structure of Iron-Containing Nanoparticles on the Functional Properties of Composite Materials Based on High-density Polyethylene’, *Russ. J. Phys. Chem. B*, vol. 16, no. 5, pp. 926–932, Oct. 2022, doi: 10.1134/S199079312205013X.

[67] M. López-R, Y. Barrios, L. D. Perez, C. Y. Soto, and C. Sierra, ‘Metal-Organic Framework (MOFs) tethered to cotton fibers display antimicrobial activity against relevant nosocomial bacteria’, *Inorganica Chimica Acta*, vol. 537, p. 120955, Jul. 2022, doi: 10.1016/j.ica.2022.120955.

[68] S. Fonseca, M.-P. Cayer, K. M. T. Ahmmed, N. Khadem-Mohtaram, S. J. Charette, and D. Brouard, ‘Characterization of the Antibacterial Activity of an SiO2 Nanoparticular Coating to Prevent Bacterial Contamination in Blood Products’, *Antibiotics*, vol. 11, no. 1, p. 107, Jan. 2022, doi: 10.3390/antibiotics11010107.

[69] P. Peer, J. Sedlaříková, M. Janalíková, L. Kučerová, and P. Pleva, ‘Novel Polyvinyl Butyral/Monoacylglycerol Nanofibrous Membrane with Antifouling Activity’, *Materials*, vol. 13, no. 17, p. 3662, Aug. 2020, doi: 10.3390/ma13173662.

[70] S. Samimi, N. Maghsoudnia, R. B. Eftekhari, and F. Dorkoosh, ‘Lipid-Based Nanoparticles for Drug Delivery Systems’, in *Characterization and Biology of Nanomaterials for Drug Delivery*, Elsevier, 2019, pp. 47–76. doi: 10.1016/B978-0-12-814031-4.00003-9.

[71] V. Selvamani, ‘Stability Studies on Nanomaterials Used in Drugs’, in *Characterization and Biology of Nanomaterials for Drug Delivery*, Elsevier, 2019, pp. 425–444. doi: 10.1016/B978-0-12-814031-4.00015-5.

[72] W. Liu, H. Lin, J. Wang, Q. Han, and F. Liu, ‘Polytetrafluoroethylene (PTFE) HFs modified by hydrophilic crosslinking network (HCN) for robust resistance to fouling and harsh chemical cleaning’, *Journal of Membrane Science*, vol. 630, p. 119301, Jul. 2021, doi: 10.1016/j.memsci.2021.119301.

[73] M. R. Mohd Ramli, A. L. Ahmad, and C. P. Leo, ‘Surface Modification of Polytetrafluoroethylene HF Membrane for Direct Contact Membrane Distillation through Low-Density Polyethylene Solution Coating’, *ACS Omega*, vol. 6, no. 7, pp. 4609–4618, Feb. 2021, doi: 10.1021/acsomega.0c05107.

[74] A. Kilic, M. Emin Karatas, L. Beyazsakal, and V. Okumus, ‘Preparation and spectral studies of boronate ester modified magnetite iron nanoparticles (Fe3O4@APTES-B) as a new type of biological agents’, *Journal of Molecular Liquids*, vol. 361, p. 119602, Sep. 2022, doi: 10.1016/j.molliq.2022.119602.

[75] D. J. Miller, D. R. Paul, and B. D. Freeman, ‘An improved method for surface modification of porous water purification membranes’, *Polymer*, vol. 55, no. 6, pp. 1375–1383, Mar. 2014, doi: 10.1016/j.polymer.2014.01.046.

[76] Z. Liu *et al.*, ‘Improvement of permeability and antifouling performance of PVDF membranes via dopamine-assisted deposition of zwitterionic copolymer’, *Colloids and Surfaces A: Physicochemical and Engineering Aspects*, vol. 656, p. 130505, Jan. 2023, doi: 10.1016/j.colsurfa.2022.130505.

[77] D. J. Miller *et al.*, ‘Short-term adhesion and long-term biofouling testing of polydopamine and poly(ethylene glycol) surface modifications of membranes and feed spacers for biofouling control’, *Water Research*, vol. 46, no. 12, pp. 3737–3753, Aug. 2012, doi: 10.1016/j.watres.2012.03.058.

[78] N. Shahkaramipour, T. Tran, S. Ramanan, and H. Lin, ‘Membranes with Surface-Enhanced Antifouling

Properties for Water Purification', *Membranes*, vol. 7, no. 1, p. 13, Mar. 2017, doi: 10.3390/membranes7010013.

[79] M. Czieborowski, A. J. B. Kemperman, E. Rolevink, J. Blom, T. Visser, and B. Philipp, 'A two-step bioluminescence assay for optimizing antibacterial coating of hollow-fiber membranes with polydopamine in an integrative approach', *Journal of Microbiological Methods*, vol. 196, p. 106452, May 2022, doi: 10.1016/j.mimet.2022.106452.

[80] H. Karkhanechi, R. Takagi, and H. Matsuyama, 'Biofouling resistance of reverse osmosis membrane modified with polydopamine', *Desalination*, vol. 336, pp. 87–96, Mar. 2014, doi: 10.1016/j.desal.2013.12.033.

[81] V. Rani, Y. Verma, and S. V. S. Rana, 'Zinc Oxide Nanoparticles Ameliorate Dimethylnitrosamine-Induced Renal Toxicity in Rat', *Appl Biochem Biotechnol*, vol. 194, no. 4, pp. 1699–1715, Apr. 2022, doi: 10.1007/s12010-021-03689-4.

[82] V. Raffa *et al.*, 'Zinc oxide nanoparticles as selective killers of proliferating cells', *IJN*, p. 1129, May 2011, doi: 10.2147/IJN.S16581.

[83] Z. Iyigundogdu *et al.*, 'Thermoplastic elastomers containing antimicrobial and antiviral additives for mobility applications', *Composites Part B: Engineering*, vol. 242, p. 110060, Aug. 2022, doi: 10.1016/j.compositesb.2022.110060.

[84] M. López-R, Y. Barrios, L. D. Perez, C. Y. Soto, and C. Sierra, 'Metal-Organic Framework (MOFs) tethered to cotton fibers display antimicrobial activity against relevant nosocomial bacteria', *Inorganica Chimica Acta*, vol. 537, p. 120955, Jul. 2022, doi: 10.1016/j.ica.2022.120955.

Curriculum Vitae

Hadi Taghavian

Education

(06.2021 – now) **PhD student**; *Technical University of Liberec, Czech Republic (www.tul.cz)*
Environmental Engineering
Dissertation title: “Highly efficient membrane development for advanced WWT system”.
Research area: water & wastewater treatment, HF membrane, MBR, surface engineering.

(09.2010 – 12.2012) **Master of Science**; *(IAU), Tehran, Iran (www.azad.ac.ir)*
Polymer Engineering
Thesis: “Producing Biocompatible NFs via Electrospinning Technique from Polymer Blends Used for Medical & Biological Applications”.

(09.2005 – 02.2010) **Bachelor of Science**; *(IAU) khuzestan, Iran (www.mahshahriau.ac.ir)*
Polymer Engineering
Final Project: “A Survey on Physical-Mechanical Properties of Rigid Polyurethane Foam”.

Professional Exp.

(Since 01.2020) **Institute for Nanomaterials, Advanced Technologies and Innovation CXI, TUL (tul.cz)**
Junior Researcher
Project title: "Ultrafiltration membrane development for WWT ".
Project title: "Hybrid material for hierarchical structure".

(05.2018 – 01.2020) **MAMMUT WORLD (https://mammutworld.com/en)**
Production department - Head of Paint-shop
Successful implementation of visual-management-dashboard in paint-shop on a basis of: Q , C, T, HR, M.
Developing and successfully implementation of SCANIA’s platform and top-coat covering of SCANIA’s cab (first time in Iran).
Process control & System Audits, implementation of the IQA (Internal Quality Audits system).
Technical problem solving and root cause analysis of paints, coatings, applying procedures and polymeric materials.

(12.2014 – 05.2018) **MAMMUT WORLD (https://mammutworld.com/en)**
Engineering department – Engineer, Supervisor
Technical support (production team, quality inspector and customers’ service).
Research & Development (polymeric moving parts and electrostatic coatings).
Documentation and determination of instructions (Production Process and QC).
Laboratory test & analysis (primary new samples of PUR/PIR foams, paint and primers).
Determination of control plans (CP) for polymeric parts, PUR/PIR foams and coatings, Process Operation Sheets (POS), Purchasing data, Man Map and 5S ref.
Determination of type, no. of layers and DFT of the coatings of steel parts in moderate (C3) and high corrosive (C5) environments.
Training course for quality inspectors and process operators.
Polymers 16, 1048-1056 (2015).

Workshops

2023	“Short Course on Nanostructured Polymer Materials”.
2023	“Summer school on membrane for water processes”.
2020	“Simultaneous dynamic-mechanical and dielectric analysis”.
2017	“SCANIA’s cabs coating – training course in Sweden”.

2017	“Paint and coating inspection course – lecturer”.
2017	“Rigid polyurethane foam specification training course”.
2016	“Paint and coating”.
2016	“17th course of composite materials & processes”.
2016	"Designation of composite structures against high velocity stress".
2015	“Polyurethane, elastomers, adhesives & foams”.
2015	“Fundamentals and principles of adhesives”.
2015	“The powder coatings: components, formulation and test methods”.
2012	“Application of polymer compounds in plastic and rubber Industries”.

Further skills and knowledge

- ISO 9001:2015 , principles and implementation procedure.
- Laboratory tests analysis: (almost all physical and mechanical test & analysis of industrial paint and coating).
- Electrostatic powder and elect./non-electrostatic liquid paints, specifications and applying procedures.
- Eminent proficiency and interested in researching and investigating to develop new materials.
- Continuous improvements, Poka-Yoke and Kaizen implementation for Process improvement.
- Root cause analysis, Pareto and fish bone diagrams for quality related problems.
- Surface preparation of: (steel parts / low surface energy of polymeric mater.) to increase adhesion bond.
- Synthesis of polymers and nanoparticles.
- Optimization and designing of experiments via RSM.

Awards

- Awarded of the *German Academic Exchange Service (DAAD)* scholarship for study in Germany.
- Awarded of the *Student Grant Scheme* from the Technical University of Liberec (SGS-2022-3037).
- Awarded the best lecture of the conference “MELPRO 2022”.